

Received September 27, 2018, accepted October 11, 2018, date of publication October 15, 2018, date of current version November 9, 2018.

Digital Object Identifier 10.1109/ACCESS.2018.2876231

Multi-Layer Downlink Precoding for Cloud-RAN Systems Using Full-Dimensional Massive MIMO

GUILLEM FEMENIAS^{ID}, (Senior Member, IEEE), AND

FELIP RIERA-PALOU^{ID}, (Senior Member, IEEE)

Mobile Communications Group, University of the Balearic Islands, 07122 Palma de Mallorca, Spain

Corresponding author: Guillem Femenias (guillem.femenias@uib.es)

This work was supported in part by the Agencia Estatal de Investigación and Fondo Europeo de Desarrollo Regional (AEI/FEDER, UE) through the Projects ELISA under Grant TEC2014-59255-C3-2-R and TERESA under Grant TEC2017-90093-C3-3-R and in part by the Ministerio de Economía y Competitividad, Spain.

ABSTRACT Full-dimensional (FD) massive multiple-input multiple-output (MIMO) has recently emerged as one of the physical layer enablers of 5G systems. Grounded on prior work on layered precoding, a novel framework for low-complexity multi-layer downlink precoding in multi-cluster cloud radio access network (C-RAN) systems using FD massive MIMO is introduced in this paper. The precoding matrix used at the cluster of remote radio heads (RRHs) associated to a given central control unit (CCU) of the C-RAN is decoupled as a multiplication of three precoding sub-matrices (or layers), a precoding architecture that leverages the special characteristics of the elevation component of the channel correlation matrix to manage both the C-RAN inter-cluster interference and the massive MIMO pilot contamination based on the availability of statistical channel state information. The proposed multi-layer approach is then adapted to the compress-after-precoding-based CCU-RRH functional split where the first and second precoding layers are locally applied at each of the RRHs in a cluster, whereas only the third precoding layer is implemented at the CCU. Optimal and suboptimal solutions are provided, which take into account both the per-RRH transmit power constraints and the capacity constraints of the fronthaul links between the CCU and the associated RRHs. The suboptimal approach, which is rooted on the vector normalization techniques used in massive MIMO precoding schemes with uniform power allocation, is shown to provide minor spectral efficiency losses when compared with the optimal solution. Numerical simulations are used to illustrate the potential of the proposed C-RAN-based framework when benchmarked against the *classical* FD massive MIMO scheme.

INDEX TERMS Multi-layer precoding, Cloud-RAN, full-dimensional MIMO, massive MIMO.

I. INTRODUCTION

Fueled by the popularity of smartphones, tablets and video streaming, modern wireless communication networks are experiencing an explosive growth of data traffic demand and there is a broad consensus in the wireless sector anticipating a plausible continuation of this trend over the years to come [1]. In order to meet this rapidly growing data volume, the wireless industry is moving towards the use of dense heterogeneous network deployments consisting of base stations (BSs) equipped with full-dimensional (FD) massive multiple-input multiple-output (MIMO) antenna configurations and covering progressively smaller service areas [2]. A dense deployment of BSs that is complemented with the installation of high-performance low-latency fronthauls connecting the

remote radio heads (RRHs) to cloud-computing based central control units (CCUs) that open up the implementation of a cloud radio access network (C-RAN) architecture with coordinated multipoint (CoMP) transmission [3].

In a C-RAN architecture, the coordination and joint signal processing across multiple BSs (or RRHs) provides a platform that, from a theoretical point of view, can potentially transform a dense inter-cell interference limited network into a near-interference-free system with almost all mobile stations (MSs) experiencing very high levels of quality of service (QoS) [4]–[8]. Network-wide multi-cell joint signal processing, however, specially when dealing with FD massive MIMO arrays of distributed antennas, place enormous capacity demands on the fronthaul links, as both data traffic

and channel state information (CSI) must be shared among all the participating nodes [4], [9]. A practical alternative to network-wide multi-cell joint signal processing can be found in the use of multi-cluster coordinated precoding strategies, particularly attractive in C-RAN-based massive MIMO scenarios where the large antenna arrays provide abundance of spatial degrees of freedoms (DoFs) that can be exploited to cancel (or reduce) the interference to MSs located in the neighboring clusters (or cells) [4], [10]–[15].

In essence, coordinated precoding strategies aim at making full use of and deriving benefit from some of the available spatial dimensions to suppress inter-cluster interference at the MSs located near the edge of neighboring clusters, and the remaining DoFs are then used to provide service to MSs located in the cluster of interest. As a by-product, most of these coordinated precoders also help canceling or reducing the detrimental effects of pilot contamination. Coordinated precoding solutions presented in [10]–[15], however, were not designed to exploit the characteristics of three-dimensional (3D) propagation channels created by the use of FD massive MIMO antenna arrays [16]–[19] and, in certain cases, still require of some form of CSI sharing among neighboring clusters. A particularly interesting precoding strategy that leverages the directional attributes of FD massive MIMO channels to control inter-cluster interference with low CSI requirements is known as layered or multi-layered downlink precoding (see, for instance, [20]–[22] and references therein). Using this approach, the precoding matrix of each BS is decoupled as a multiplication of different matrices, denoted as layers, which are specifically designed to cope with different sources of interference, with low channel estimation training overhead and allowing for the implementation of efficient and low-complexity hybrid analog/digital architectures [20], [21], [23]–[26]. Interestingly, Kang *et al.* [25], [26] propose a layered downlink precoding scheme for C-RAN systems with FD-MIMO. The proposed solutions leverage the special characteristics of the 3D MIMO channels to control the fronthaul overhead generated by the transmission of baseband signals from the CCU to the associated RRHs. However, the proposed layered precoders are designed assuming a single-cluster C-RAN and thus, do not take into account the effects of out-of-cluster interference, which ultimately limit the performance of these systems. Moreover, the complexity of the proposed optimization approach makes it difficult, if at all possible, to obtain similar designs that can be effectively applied to massive MIMO-based C-RAN networks.

Motivated by the above discussion, our main aim in this paper is to address the design and performance analysis of a multi-clustered C-RAN using FD massive MIMO that, grounded on previous work on multi-layer precoding, takes full advantage of the particular attributes of 3D massive MIMO channels to control both the inter-cluster interference and the capacity demands on the fronthaul links. In particular, this work seeks to highlight the potential benefits C-RAN can bring along while taking into account the infrastructure

requirements. The main contributions of our work can be summarized as follows:

- Extending the work by Alkhateeb *et al.* [21], a low-complexity multi-layer precoding scheme is proposed whereby the cluster-based precoding matrix at each CCU of the C-RAN is decoupled as a multiplication of three precoding layers. Aiming at adapting the proposed multi-layer precoder to the C-RAN scenario, a refinement of the compress-after-precoding (CAP)-based [25], [27] CCU-RRH functional split is presented where the first and second precoding layers are locally applied at each of the RRHs, whereas only the third precoding layer is implemented at the CCU, thus achieving full RRH cooperation with a low implementation complexity and reduced CSI feedback requirements between the RRHs and the CCU. In sharp contrast to the centralized scheme proposed by Alkhateeb *et al.* [21], implementing a precoding matrix that is distributed between the CCU and the RRHs it controls requires of: (i) considering the per-RRH power limitations, (ii) designing precoders that allow the first and second precoding layers to be distributed among the different RRHs, and (iii) forwarding a compressed (and thus distorted) version of the third-layer beamformed signal to the associated RRHs through the limited-capacity fronthaul links.
- The design of multi-layer downlink precoders in multi-clustered C-RAN systems using FD massive MIMO is then formulated as an optimization problem with constraints on both the per-RRH transmit power and the per-fronthaul capacity. It is shown that this is a non-convex optimization problem that can only be tackled using global optimization algorithms. The complexity of the global optimization approach, however, makes it far from practical and hence, rooted on the vector normalization techniques used in massive MIMO precoding schemes with uniform power allocation [28], a feasible suboptimal heuristic algorithm is proposed that is shown to suffer from minor performance losses when compared to the optimal solution at an affordable computational complexity.
- The proposed optimization approach is thoroughly evaluated through numerical simulations and benchmarked against a *classical* multi-layer FD massive MIMO scheme with a single BS per cell (no clusterization) and without the limitations associated with finite-capacity fronthauling. Numerical results reveal that, assuming CCU-RRH fronthaul links of sufficient capacity, the proposed C-RAN-based approach achieves clear spectral efficiency gains with respect to the *classical* non-cooperative multi-cell FD massive MIMO scheme. Interestingly, the proposed framework allows an accurate quantification of the fronthaul requirements, thus permitting the network designer to adequately balance the tradeoff between infrastructure demands and performance improvement. Moreover, as the number of RRHs per cluster increases, the proposed C-RAN-based

strategy improves the QoS experienced by the MSs located near the cluster edge, thus increasing the spectral efficiency fairness among users across the cluster.

The remainder of this paper is organized as follows. In Section II the system model under consideration is introduced. The proposed adaptation of the multi-layer precoding approach to a C-RAN scenario is presented in Section III where the peculiarities associated to the use of a CAP-based CCU-RRH functional split are fully taken into account. Globally optimal and feasible suboptimal heuristic solutions to design the multi-layer downlink precoders are proposed in Section IV. Numerical results are provided in V and, finally, concluding remarks are summarized in Section VI.

Notation: Vectors and matrices are denoted by lower-case and upper-case boldface symbols. The q -dimensional identity matrix is represented by \mathbf{I}_q . The operator $\det(\mathbf{X})$ represents the determinant of matrix \mathbf{X} , $\text{rank}(\mathbf{X})$ is its rank, $\|\mathbf{X}\|_F$ is its Frobenius norm, whereas \mathbf{X}^{-1} , \mathbf{X}^T , \mathbf{X}^* and \mathbf{X}^H denote its inverse, transpose, conjugate and conjugate transpose (also known as Hermitian), respectively. The operator $\text{diag}(\mathbf{x})$ is used to denote a diagonal with the entries of vector \mathbf{x} on its main diagonal. The Kronecker product of \mathbf{X} and \mathbf{Y} is represented as $\mathbf{X} \otimes \mathbf{Y}$. Finally, $\mathcal{N}(\mathbf{m}, \mathbf{R})$ and $\mathcal{CN}(\mathbf{m}, \mathbf{R})$ represent the real and complex Gaussian vector distributions with mean \mathbf{m} and covariance \mathbf{R} , respectively.

II. SYSTEM MODEL

As schematically shown in Fig. 1, let us consider the downlink of a C-RAN with N_C mutually interfering clusters of RRHs. The clusters are indexed by the set $\mathcal{N}_C = \{1, \dots, N_C\}$ and cluster $c \in \mathcal{N}_C$ has a single CCU that controls N_{Rc} RRHs indexed by the set $\mathcal{N}_{Rc} = \{1, \dots, N_{Rc}\}$. The c th CCU communicates with the r th RRH through a fronthaul link of capacity $\bar{C}_{c,r}$ bit/s/Hz and connects to the a generic core network via the backhaul. The r th RRH of cluster c is equipped with a two-dimensional (2D) uniform rectangular array (URA) with $n_{Tc,r} = n_{Tc,r}^A n_{Tc,r}^E$ elements, where $n_{Tc,r}^A$ and $n_{Tc,r}^E$ denote the number of antennas in the azimuth- and elevation-domains, respectively. The N_{Rc} RRHs in cluster c are used to provide service to N_{Mc} single-antenna MSs indexed by the set $\mathcal{N}_{Mc} = \{1, \dots, N_{Mc}\}$. It is assumed that all RRHs and MSs are synchronized and use a time division duplexing (TDD) protocol with universal frequency reuse.

A. SIGNAL MODEL

Let us define $\mathbf{s}_{c'} = [s_{c',1} \dots s_{c',N_{Mc'}}]^T$ as the $N_{Mc'} \times 1$ vector of symbols jointly (cooperatively) transmitted from the RRHs in cluster $c' \in \mathcal{N}_C$ to the MSs in $\mathcal{N}_{Mc'}$, such that $E\{\mathbf{s}_{c'} \mathbf{s}_{c'}^H\} = \mathbf{I}_{N_{Mc'}}$. Let us also define $\mathbf{x}_{c',r} = \mathcal{P}_{c',r}(\mathbf{s}_{c'})$ as the $n_{Tc',r} \times 1$ vector of signals transmitted from the r th RRH in cluster $c' \in \mathcal{N}_C$, where $\mathcal{P}_{c',r}(\mathbf{s}_{c'})$ is used to denote the mathematical operations (linear and/or non-linear) used to obtain $\mathbf{x}_{c',r}$ from $\mathbf{s}_{c'}$. Note that this vector must comply with a power constraint $\mathbb{E}\{\|\mathbf{x}_{c',r}\|^2\} \leq \bar{P}_{c',r}$, where $\bar{P}_{c',r}$ is the

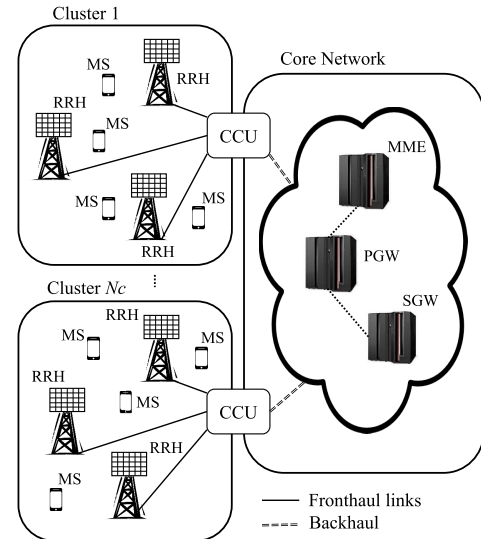


FIGURE 1. System model: network topology.

maximum transmit power available at RRH r in cluster c' . Assuming that the uplink and downlink channels are reciprocal, if $\mathbf{h}_{c,m}^{c',r}$ denotes the $n_{Tc',r} \times 1$ uplink channel from MS m in cluster c to RRH r in cluster c' , then the signal received by this MS can be expressed as

$$y_{c,m} = \sum_{c'=1}^{N_C} \mathbf{h}_{c,m}^{c',r} \mathbf{x}_{c'} + n_{c,m}, \quad (1)$$

where $n_{c,m} \sim \mathcal{CN}(0, \sigma_n^2)$ is the Gaussian noise sample at MS m in cell c , $\mathbf{h}_{c,m}^{c',r} = [\mathbf{h}_{c,m}^{c',1T} \dots \mathbf{h}_{c,m}^{c',N_{Rc'}T}]^T$ denotes the joint uplink channel vector from the m th MS in cluster c to all the RRHs in cluster c' , and $\mathbf{x}_{c'} = [\mathbf{x}_{c',1}^T \dots \mathbf{x}_{c',N_{Rc'}}^T]^T$ is the vector of signals jointly (cooperatively) transmitted from all the RRHs in cluster c' . The vector $\mathbf{y}_c = [y_{c,1} \dots y_{c,N_{Mc}}]^T$ containing the signals received by the N_{Mc} scheduled MSs in cluster c can then be expressed as

$$\mathbf{y}_c = \sum_{c'=1}^{N_C} \mathbf{H}_c^{c',r} \mathbf{x}_{c'} + \mathbf{n}_c, \quad (2)$$

where $\mathbf{H}_c^{c'} = [\mathbf{h}_{c,1}^{c'} \dots \mathbf{h}_{c,N_{Mc}}^{c'}]^T$ and $\mathbf{n}_c = [n_{c,1} \dots n_{c,N_{Mc}}]^T$.

B. CHANNEL MODEL

Assuming that the MS is sufficiently far away from the RRHs, a condition easily fulfilled in practice, the channel $\mathbf{h}_{c,m}^{c',r}$ can be safely modeled through the use of a Kronecker product spatial correlation model [17], [21]. In this model, the covariance matrix of the 3D channel $\mathbf{h}_{c,m}^{c',r}$ can be approximated as

$$\mathbf{R}_{c,m}^{c',r} = E\{\mathbf{h}_{c,m}^{c',r} \mathbf{h}_{c,m}^{c',rH}\} \approx \mathbf{R}_{c,m}^{c',rA} \otimes \mathbf{R}_{c,m}^{c',rE}, \quad (3)$$

where, using the (reduced) eigenvalue decomposition, the covariance matrices in the azimuth and elevation

directions can be expressed as

$$\begin{aligned}\mathbf{R}_{c,m}^{c',rA} &= \mathbf{U}_{c,m}^{c',rA} \Lambda_{c,m}^{c',rA} \mathbf{U}_{c,m}^{c',rA H}, \\ \mathbf{R}_{c,m}^{c',rE} &= \mathbf{U}_{c,m}^{c',rE} \Lambda_{c,m}^{c',rE} \mathbf{U}_{c,m}^{c',rE H},\end{aligned}\quad (4)$$

with $\mathbf{U}_{c,m}^{c',rA}$ and $\mathbf{U}_{c,m}^{c',rE}$ denoting, respectively, the $n_T^{c',r} \times r_{c,m}^{c',rA}$ and $n_T^{c',r} \times r_{c,m}^{c',rE}$ matrices of eigenvectors and $\Lambda_{c,m}^{c',rA}$ and $\Lambda_{c,m}^{c',rE}$ denoting square diagonal matrices containing the $r_{c,m}^{c',rA}$ and $r_{c,m}^{c',rE}$ non-null eigenvalues in their main diagonals. Using these (reduced) eigenvalue decompositions, the channel $\mathbf{h}_{c,m}^{c',r}$ can be expressed as (see [22, Sec. 3.1.2] and references therein)

$$\mathbf{h}_{c,m}^{c',r} = \left(\mathbf{U}_{c,m}^{c',rA} \Lambda_{c,m}^{c',rA^{\frac{1}{2}}} \otimes \mathbf{U}_{c,m}^{c',rE} \Lambda_{c,m}^{c',rE^{\frac{1}{2}}} \right) \mathbf{z}_{c,m}^{c',r}, \quad (5)$$

where $\mathbf{z}_{c,m}^{c',r} \sim \mathcal{CN}\left(\mathbf{0}, 10^{-PL_{c,m}^{c',r}/10} \mathbf{I}_{r_{c,m}^{c',rA} r_{c,m}^{c',rE}}\right)$, with $PL_{c,m}^{c',r}$ denoting the propagation losses (including transmit and receive antenna gains and shadow fading) between MS m in cluster c and RRH r in cluster c' .

III. MULTI-LAYER PRECODING IN A C-RAN

A. MIMO PRECODING AND FRONTHAUL COMPRESSION

The mathematical operations that symbol vector $s_{c'}$ undergoes before being transmitted, generically represented as $\mathbf{x}_{c',r} = \mathcal{P}_{c',r}(s_{c'})$, for all $r \in \mathcal{N}_{R_{c'}}$, include, on the one hand, a MIMO precoding task and, on the other hand, a compressing process of all or part of the data that must be sent from the CCU to the RRHs through the fronthaul links. Designing the MIMO precoding matrices with the objective of, for instance, maximizing the system sum-rate, with constraints on the amount of power that can be transmitted from each of the RRHs in the network and considering the non-linear effects of the compression processes, leads to non-convex optimization problems whose closed-form solution is unknown [4]. Also, inter-cluster interference coordination typically entails a prohibitive coordination overhead that limits the pursued value of cooperation [9]. This latter issue is even more exacerbated when dealing with C-RAN scenarios in which coordination information has to be transferred not only among the CCUs controlling the different clusters of RRHs but also among each of the CCUs and the RRHs they control. In trying to deal with these issues, multi-layer precoding techniques leveraging the channel decomposition resulting from the Kronecker channel model introduced in (3) have been proposed in the literature [21], [26], [29].

As in the work by Alkhateeb *et al.* [21], a three-layer MIMO precoding matrix will be considered in this paper. Furthermore, aiming at adapting this layered scheme to the C-RAN scenario, a modification of the CAP-based [25], [27] (also known as compression strategy [30])¹

¹The application of the compress-before-precoding (CBP)-based scheme [25] (also known as data-sharing strategy [30]) to this scenario is left for further research.

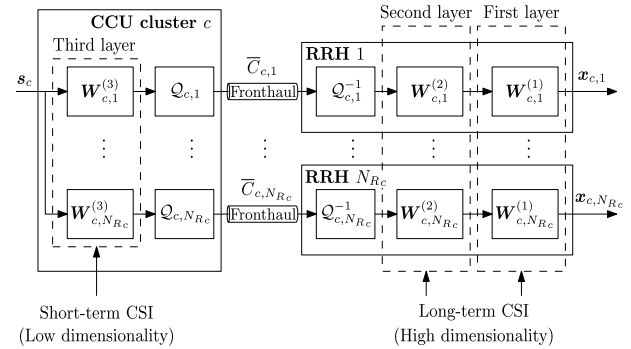


FIGURE 2. Block diagram of the layered CAP scheme.

CCU-RRH functional split will be studied. As shown in Fig. 2, in the proposed layered CAP strategy, the first and second precoding layers will be locally applied at each of the RRHs in a cluster, whereas the third layer precoding process will be performed centrally at the CCU and a compressed version of the first-layer beamformed signal will then be forwarded to the RRHs through the fronthaul links. As will be shown next, layered precoding allows leveraging the directional characteristics of 3D MIMO channels to efficiently manage inter-cluster interference using long-term statistical CSI. Furthermore, one of the advantages of the CAP-based approach in front of other CCU-RRH functional splits is that, since the CCU has complete access to user data, it can achieve full RRH cooperation. Compressing the precoded signals, however, introduces distortion in the form of quantization noise that has to be taken into account when deriving the performance of this layered precoding/compression strategy.

Let us denote by $\mathcal{Q}_{c',r}(\mathbf{x})$ and $\mathcal{Q}_{c',r}^{-1}(\mathbf{x})$ the quantization and unquantization mathematical operations performed by the layered CAP-based CCU-RRH functional split on a vector of signal samples \mathbf{x} to be transmitted by RRH r in cluster c' . Due to the distortion introduced by the quantization/unquantization processes, we have that [31]

$$\hat{\mathbf{x}}_{c',r}(\mathbf{x}) \triangleq \mathcal{Q}_{c',r}^{-1}(\mathcal{Q}_{c',r}(\mathbf{x})) = \mathbf{x} + \mathbf{q}_{c',r}, \quad (6)$$

where $\mathbf{q}_{c',r}$ is the quantization noise vector, which is assumed to be statistically distributed as $\mathbf{q}_{c',r} \sim \mathcal{CN}\left(\mathbf{0}, \sigma_{q_{c',r}}^2 \mathbf{I}\right)$. As shown by Zamir and Feder [31], this assumption is supported by the fact that large-block lattice quantization codes are able to approximate a Gaussian quantization noise distribution. Thus, the mathematical operations describing the CCU-RRH functional split considered in this paper can be summarized as

$$\begin{aligned}\mathbf{x}_{c',r} &= \mathcal{P}_{c',r}(s_{c'}) = \mathbf{W}_{c',r}^{(1)} \mathbf{W}_{c',r}^{(2)} \hat{\mathcal{Q}}_{c',r} \left(\mathbf{W}_{c',r}^{(3)} s_{c'} \right) \\ &= \mathbf{W}_{c',r}^{(1)} \mathbf{W}_{c',r}^{(2)} \left(\mathbf{W}_{c',r}^{(3)} s_{c'} + \mathbf{q}_{c',r} \right),\end{aligned}\quad (7)$$

where $\mathbf{W}_{c',r}^{(i)}$ denotes the i th layer precoding matrix at the r th RRH. The power transmitted by RRH r in

cluster c' can then be computed as

$$P_{Tc',r} = \left\| \mathbf{W}_{c',r}^{(1)} \mathbf{W}_{c',r}^{(2)} \mathbf{W}_{c',r}^{(3)} \right\|_F^2 + \sigma_{q_{c',r}}^2 \left\| \mathbf{W}_{c',r}^{(1)} \mathbf{W}_{c',r}^{(2)} \right\|_F^2. \quad (8)$$

Assuming that the transmit power available at the r th RRH in cluster c' is $\bar{P}_{c',r}$, the per-RRH power constraint $P_{Tc',r} \leq \bar{P}_{c',r}$ must be fulfilled for all $r \in \mathcal{N}_{Rc'}$.

Using the proposed three-layer CAP approach, the signal received by MS m in cluster c can be rewritten as

$$\begin{aligned} y_{c,m} &= \sum_{r=1}^{N_{Rc}} \mathbf{h}_{c,m}^{c,r T} \mathbf{W}_{c,r}^{(1)} \mathbf{W}_{c,r}^{(2)} \mathbf{W}_{c,r}^{(3)} s_c \\ &\quad + \sum_{\substack{c'=1 \\ c' \neq c}}^{N_C} \sum_{r=1}^{N_{Rc'}} \mathbf{h}_{c,m}^{c',r T} \mathbf{W}_{c',r}^{(1)} \mathbf{W}_{c',r}^{(2)} \mathbf{W}_{c',r}^{(3)} s_{c'} + \eta_{c,m}, \end{aligned} \quad (9)$$

where the first term is the desired received signal from the RRHs serving cluster c , the second term is the received signal from RRHs located in other clusters (inter-cluster interference), and the third term, defined as

$$\eta_{c,m} = \sum_{c'=1}^{N_C} \sum_{r=1}^{N_{Rc'}} q_{c',m}^{c',r} + n_{c,m}, \quad (10)$$

with $q_{c',m}^{c',r} = \mathbf{h}_{c,m}^{c',r T} \mathbf{W}_{c',r}^{(1)} \mathbf{W}_{c',r}^{(2)} \mathbf{q}_{c',r}$, includes the thermal noise as well as the quantization noise samples received from all the RRHs in the network.

B. FIRST LAYER: AVOIDING INTER-CLUSTER INTERFERENCE

In order to avoid the inter-cluster interference, the first layer precoding matrices $\mathbf{W}_{c',r}^{(1)}$, for $r \in \{1, \dots, N_{Rc'}\}$, must be designed in such a way that the second term in the right hand side (RHS) of (9) is cancelled. Leveraging the Kronecker channel model described in (3), the first layer precoding matrices are structured as

$$\mathbf{W}_{c',r}^{(1)} = \mathbf{W}_{c',r}^{(1)A} \otimes \mathbf{W}_{c',r}^{(1)E}. \quad (11)$$

Thus, adopting the channel model in (5), the terms $\mathbf{h}_{c,m}^{c',r T} \mathbf{W}_{c',r}^{(1)}$ in (9), for all $r \in \mathcal{N}_{Rc'}$, can be expanded as

$$\mathbf{h}_{c,m}^{c',r T} \mathbf{W}_{c',r}^{(1)} = \bar{\mathbf{z}}_{c,m}^{c',r T} \left(\mathbf{U}_{c,m}^{c',r A T} \mathbf{W}_{c',r}^{(1)A} \otimes \mathbf{U}_{c,m}^{c',r E T} \mathbf{W}_{c',r}^{(1)E} \right), \quad (12)$$

where $\bar{\mathbf{z}}_{c,m}^{c',r} = \left(\Lambda_{c,m}^{c',r A \frac{1}{2}} \otimes \Lambda_{c,m}^{c',r E \frac{1}{2}} \right) \mathbf{z}_{c,m}^{c',r}$. Hence, inter-cluster interference can be avoided by designing $\mathbf{W}_{c',r}^{(1)}$ in such a way that either $\mathbf{U}_{c,m}^{c',r A T} \mathbf{W}_{c',r}^{(1)A} = \mathbf{0}$ or $\mathbf{U}_{c,m}^{c',r E T} \mathbf{W}_{c',r}^{(1)E} = \mathbf{0}$, for all $c' \neq c$ and all $r \in \mathcal{N}_{Rc'}$. In the same manner, for any RRH r in cluster c to avoid interfering users located in other clusters, it has to use either a precoding matrix $\mathbf{W}_{c,r}^{(1)A}$ transmitting on the null-space of the azimuth covariance matrices of all the channels between this RRH

and all the users in other clusters and/or a precoding matrix $\mathbf{W}_{c,r}^{(1)E}$ transmitting on the null-space of the corresponding set of elevation covariance matrices. That is, either $\mathbf{W}_{c,r}^{(1)A}$ must be in Null $\left(\sum_{c' \neq c} \sum_{m'=1}^{N_{M_c'}} \mathbf{R}_{c',m'}^{c,r} \right)$ or $\mathbf{W}_{c,r}^{(1)E}$ must be in Null $\left(\sum_{c' \neq c} \sum_{m'=1}^{N_{M_c'}} \mathbf{R}_{c',m'}^{c,r} \right)$.

As reported by Ying *et al.* [17], full-dimensional MIMO (FD-MIMO) channels exhibit time variability at very different timescales for both azimuth and elevation directions, with the elevation component varying at a significantly slower pace than the azimuth one. Leveraging the dynamic characteristics of these channels, the inter-cluster interference will be managed in the elevation direction by setting

$$\mathbf{W}_{c,r}^{(1)A} = \mathbf{I}_{n_{Tc,r}^A}, \quad (13)$$

and designing the elevation component such that $\mathbf{W}_{c,r}^{(1)E}$ is in Null $\left(\sum_{c' \neq c} \sum_{m'=1}^{N_{M_c'}} \mathbf{R}_{c',m'}^{c,r} \right)$. Furthermore, since the elevation direction is typically subject to small scattering [32], [33], the use of 2D antenna arrays with a large number of vertical elements results in low-rank covariance matrices in this direction. This means that the null-space of different scheduled users will typically exhibit a large overlap and hence, designing the precoding matrix $\mathbf{W}_{c,r}^{(1)E}$ to be in Null $\left(\sum_{c' \neq c} \sum_{m'=1}^{N_{M_c'}} \mathbf{R}_{c',m'}^{c,r} \right)$ is in practice equivalent² to design it to be in Null $\left(\bar{\mathbf{R}}_{c,r}^E \right)$, where

$$\bar{\mathbf{R}}_{c,r}^E = \sum_{c' \neq c} E_{\mathcal{N}_{M_c'}} \left\{ \mathbf{R}_{c',m'}^{c,r} \right\} \quad (14)$$

is defined as the average interference covariance matrix in the elevation direction for RRH r in cluster c [21]. The eigen-decomposition of $\bar{\mathbf{R}}_{c,r}^E$ can be expressed as

$$\bar{\mathbf{R}}_{c,r}^E = \left[\mathbf{D}_{c,r} \mathbf{D}_{c,r}^0 \right] \Delta_{c,r} \left[\mathbf{D}_{c,r} \mathbf{D}_{c,r}^0 \right]^H, \quad (15)$$

where, assuming that $\text{rank}[\bar{\mathbf{R}}_{c,r}^E] = r_{c,r}^E$, the $n_{Tc,r}^E \times r_{c,r}^E$ and $n_{Tc,r}^E \times (n_{Tc,r}^E - r_{c,r}^E)$ matrices $\mathbf{D}_{c,r}$ and $\mathbf{D}_{c,r}^0$ contain the eigenvectors corresponding to the non-null and null eigenvalues, respectively. Thus, the first precoding layer of the elevation direction is designed to be in the null-space of $\bar{\mathbf{R}}_{c,r}^E$ by

²Let us prove that for two generic covariance matrices $\mathbf{R}_1 \in \mathbb{C}^{N \times N}$ and $\mathbf{R}_2 \in \mathbb{C}^{N \times N}$, designing a precoder $\mathbf{W} \in \mathbb{C}^{N \times M}$ to be in Null (\mathbf{R}_s) , with $\mathbf{R}_s = \mathbf{R}_1 + \mathbf{R}_2 \in \mathbb{C}^{N \times N}$ and $M = \text{nullity}(\mathbf{R}_s) \leq N$, ensures that \mathbf{W} is in the null space of both \mathbf{R}_1 and \mathbf{R}_2 . Since $\mathbf{W} = [\mathbf{w}_1 \dots \mathbf{w}_M]$ is in the null space of \mathbf{R}_s , every beamforming column vector \mathbf{w}_m satisfies the condition $\mathbf{w}_m^H \mathbf{R}_s \mathbf{w}_m = \mathbf{w}_m^H \mathbf{R}_1 \mathbf{w}_m + \mathbf{w}_m^H \mathbf{R}_2 \mathbf{w}_m = 0$. Now, considering that covariance matrices \mathbf{R}_1 and \mathbf{R}_2 are positive semidefinite, we have that $\mathbf{w}_m^H \mathbf{R}_1 \mathbf{w}_m = 0$ and $\mathbf{w}_m^H \mathbf{R}_2 \mathbf{w}_m = 0$, which guarantees that the precoding matrix \mathbf{W} is in the null space of \mathbf{R}_1 and \mathbf{R}_2 .

The average of the interference covariance matrix is obtained by adding the covariance matrices experienced by different scheduled interfering MSs over different time slots. As the first layer precoding matrix obtained in a given time slot is applied to a subset of the MSs involved in the calculation of the average interference covariance matrix, designing the first layer precoding matrix to be in the null space of $\bar{\mathbf{R}}_{c,r}^E$ guarantees the complete elimination of the intercluster interference and hence, of the pilot contamination.

setting

$$\mathbf{W}_{c,r}^{(1)E} = \mathbf{D}_{c,r}^0. \quad (16)$$

With $\mathbf{W}_{c,r}^{(1)} = \mathbf{I}_{n_{Tc,r}} \otimes \mathbf{D}_{c,r}^0$, for all $c \in \mathcal{N}_C$, the inter-cluster interference is cancelled and, furthermore, as a by-product of the selected design, most of the quantization noise samples are also neutralized. Consequently, the signal received by MS m in cluster c can be rewritten as

$$y_{c,m} = \sum_{r=1}^{N_{Rc}} \bar{\mathbf{z}}_{c,m}^{c,r T} \bar{\mathbf{U}}_{c,r,m} \mathbf{W}_{c,r}^{(2)} \mathbf{W}_{c,r}^{(3)} \mathbf{s}_c + \eta_{c,m}, \quad (17)$$

where

$$\bar{\mathbf{U}}_{c,r,m} = (\mathbf{U}_{c,m}^{c,r A T} \otimes \mathbf{U}_{c,m}^{c,r E T} \mathbf{D}_{c,r}^0), \quad (18)$$

and

$$\eta_{c,m} = \sum_{r=1}^{N_{Rc}} \bar{\mathbf{z}}_{c,m}^{c,r T} \bar{\mathbf{U}}_{c,r,m} \mathbf{W}_{c,r}^{(2)} \mathbf{q}_{c,r} + n_{c,m}. \quad (19)$$

Note that only the knowledge of the long-term average interference covariance matrices $\bar{\mathbf{R}}_{c,r}^E$ (or equivalently, the subspace spanned by these matrices [21], [34]) is required to design the first precoding layer and, thus, updates of this precoder will only be necessary every long period of time. Furthermore, as demonstrated in [34], practical methods exist to conduct this channel covariance estimation virtually without error (i.e., results obtained using the practical algorithm proposed by Haghighatshoar and Caire [34] cannot be distinguished from those obtained using perfect CSI).

C. SECOND LAYER: CONJUGATE BEAMFORMING

After cancelling the inter-cluster interference, the signal vector received by the N_{Mc} MSs scheduled in cluster c can be expressed as

$$\mathbf{y}_c = \sum_{r=1}^{N_{Rc}} \begin{bmatrix} \bar{\mathbf{z}}_{c,1}^{c,r T} \bar{\mathbf{U}}_{c,r,1} \\ \vdots \\ \bar{\mathbf{z}}_{c,N_{Mc}}^{c,r T} \bar{\mathbf{U}}_{c,r,N_{Mc}} \end{bmatrix} \mathbf{W}_{c,r}^{(2)} \mathbf{W}_{c,r}^{(3)} \mathbf{s}_c + \eta_c. \quad (20)$$

Thus, as suggested by Alkhateeb *et al.* [21], aiming at focusing the transmitted power on the effective subspaces (including the first precoding layers) of the N_{Mc} MSs scheduled in cluster c , the second precoding layer can be designed as an $n_{Tc,r}^A (n_{Tc,r}^E - \bar{r}_{c,r}^E) \times \sum_{m=1}^{N_{Mc}} r_{c,m}^{c,r A} r_{c,m}^{c,r E}$ large-scale conjugate beamforming matrix

$$\mathbf{W}_{c,r}^{(2)} = [\bar{\mathbf{U}}_{c,r,1}^H \cdots \bar{\mathbf{U}}_{c,r,N_{Mc}}^H], \quad (21)$$

resulting in a received signal vector

$$\mathbf{y}_c = \sum_{r=1}^{N_{Rc}} \bar{\mathbf{H}}_{c,r}^H \mathbf{W}_{c,r}^{(3)} \mathbf{s}_c + \eta_c, \quad (22)$$

where

$$\bar{\mathbf{H}}_{c,r} = \begin{bmatrix} \bar{\mathbf{U}}_{c,r,1} \\ \vdots \\ \bar{\mathbf{U}}_{c,r,N_{Mc}} \end{bmatrix} [\bar{\mathbf{U}}_{c,r,1}^H \bar{\mathbf{z}}_{c,1}^{c,r} \cdots \bar{\mathbf{U}}_{c,r,N_{Mc}}^H \bar{\mathbf{z}}_{c,N_{Mc}}^{c,r}], \quad (23)$$

and the quantization/thermal noise samples reduce to

$$\eta_{c,m} = \sum_{r=1}^{N_{Rc}} \bar{\mathbf{h}}_{c,r,m} \mathbf{q}_{c,r} + n_{c,m}. \quad (24)$$

where $\bar{\mathbf{h}}_{c,r,m}$ is the m th column of $\bar{\mathbf{H}}_{c,r}$.

Again, updating the second precoding layer will only be required every long period of time as it is solely based on the knowledge of the large-scale matrices $\bar{\mathbf{U}}_{c,r,m}$ defined in (18) that, as suggested by Alkhateeb *et al.* [21], can be efficiently obtained using subspace estimation techniques [34]. This precoding layer can be interpreted as a long-term CSI-based *statistical* matched filter that, apart from focusing the transmitted power on the effective subspaces of the scheduled MSs, also serves to decrease the dimensionality of the resulting equivalent MIMO channel, thus reducing the complexity of the sort-term CSI-based third precoding layer.

D. THIRD LAYER: MANAGING THE MULTI-USER INTERFERENCE

Finally, intra-cluster multi-user interference can be effectively cancelled by implementing a third-layer zero-forcing (ZF) precoding matrix

$$\mathbf{W}_c^{(3)} = \begin{bmatrix} \bar{\mathbf{W}}_{c,1}^{(3)} \\ \vdots \\ \bar{\mathbf{W}}_{c,N_{Rc}}^{(3)} \end{bmatrix} \boldsymbol{\Upsilon}_c^{\frac{1}{2}} = \bar{\mathbf{H}}_c \left(\bar{\mathbf{H}}_c^H \bar{\mathbf{H}}_c \right)^{-1} \boldsymbol{\Upsilon}_c^{\frac{1}{2}}, \quad (25)$$

where $\bar{\mathbf{H}}_c = [\bar{\mathbf{H}}_{c,1}^T \cdots \bar{\mathbf{H}}_{c,N_{Rc}}^T]^T$ is the equivalent MIMO channel (after first and second layer precoding) experienced by the CCU in cluster c , and $\boldsymbol{\Upsilon}_c = \text{diag}(\nu_{c,1} \dots \nu_{c,N_{Mc}})$ is used to guarantee that the global precoding matrix fulfills the transmit power constraints on each of the RRHs in cluster c .

The received signal sample at MS m in cluster c is

$$y_{c,m} = \sqrt{\nu_{c,m}} s_{c,m} + \eta_{c,m}, \quad (26)$$

resulting in an estimated signal-to-interference-plus-noise ratio (SINR) that can be expressed as

$$\text{SINR}_{c,m} = \frac{\nu_{c,m}}{\sum_{r=1}^{N_{Rc}} \sigma_{q_{c,r}}^2 \|\bar{\mathbf{h}}_{c,r,m}\|^2 + \sigma_n^2}, \quad (27)$$

where it has been assumed, as in [21], that a perfect CSI is available at the MSs.

As a result of the joint effects of the first and second precoding layers, first, the pilot contamination has been virtually cancelled and, second, the dimensionality of the equivalent MIMO channel $\bar{\mathbf{H}}_c$ is expected to be much smaller than

the original massive MIMO channel. These effects allow the practical use of uplink and downlink pilots for short-term instantaneous channel estimation at both the RRHs and the MSs. Analyzing the effects produced by non-ideal pilot contamination cancellation and/or imperfect instantaneous channel estimation processes is beyond the scope of this paper and thus left for further research.

It is worth noting that despite more complex precoders could be used in this layer (e.g., regularized zero forcing/minimum mean square error (RZF/MMSE), dirty paper coding/ successive interference cancellation (DPC/SIC)), as pointed out in [35], the simple ZF precoder quickly approaches capacity as the number of transmit antennas increases while avoiding the exchange of information between the APs and the MSs.³

E. ACHIEVABLE RATE AND FRONTHAUL CAPACITY CONSUMPTION

Considering the system model described in Section II, the estimated achievable rate by MS m in cell c is given by

$$R_{c,m} = \log_2 \left(1 + \frac{v_{c,m}}{\sum_{r=1}^{N_{Rc}} \sigma_{q_{c,r}}^2 \|\bar{\mathbf{h}}_{c,r,m}\|^2 + \sigma_n^2} \right). \quad (28)$$

Furthermore, using (7), the quantization process performed at RRH r in cluster c can be expressed as

$$\hat{\mathcal{Q}}_{c,r}(\mathbf{W}_{c,r}^{(3)} \mathbf{s}_c) = \mathbf{W}_{c,r}^{(3)} \mathbf{s}_c + \mathbf{q}_{c,r}. \quad (29)$$

From standard random coding arguments [36], vector \mathbf{s}_c can be safely assumed to be distributed as $\mathbf{s}_c \sim \mathcal{CN}(0, \mathbf{I}_{N_{M_c}})$ and thus, the quantized vector $\hat{\mathcal{Q}}_{c,r}(\mathbf{W}_{c,r}^{(3)} \mathbf{s}_c)$ is distributed as $\hat{\mathcal{Q}}_{c,r}(\mathbf{W}_{c,r}^{(3)} \mathbf{s}_c) \sim \mathcal{CN}\left(0, \|\mathbf{W}_{c,r}^{(3)}\|^2 + \sigma_{q_{c,r}}^2 \mathbf{I}_{r_{c,r}}\right)$. Furthermore, as the differential entropy of a vector $\mathbf{x} \sim \mathcal{CN}(\boldsymbol{\mu}, \boldsymbol{\Theta})$ is given by $\mathcal{H}(\mathbf{x}) = \log \det(\pi e \boldsymbol{\Theta})$ [36], the required rate to transfer the quantized vector $\hat{\mathcal{Q}}_{c,r}(\mathbf{W}_{c,r}^{(3)} \mathbf{s}_c)$ on the corresponding fronthaul link can be obtained as (in bps/Hz)

$$\begin{aligned} \hat{C}_{c,r} &= I\left(\hat{\mathcal{Q}}_{c,r}(\mathbf{W}_{c,r}^{(3)} \mathbf{s}_c); \mathbf{W}_{c,r}^{(3)} \mathbf{s}_c\right) \\ &= \mathcal{H}\left(\hat{\mathcal{Q}}_{c,r}(\mathbf{W}_{c,r}^{(3)} \mathbf{s}_c)\right) - \mathcal{H}\left(\hat{\mathcal{Q}}_{c,r}(\mathbf{W}_{c,r}^{(3)} \mathbf{s}_c) | \mathbf{W}_{c,r}^{(3)} \mathbf{s}_c\right) \\ &= \log_2 \det\left(\|\mathbf{W}_{c,r}^{(3)}\|^2 + \sigma_{q_{c,r}}^2 \mathbf{I}_{r_{c,r}}\right) - r_{c,r} \log_2\left(\sigma_{q_{c,r}}^2\right), \end{aligned} \quad (30)$$

where $I(\hat{\mathbf{x}}; \mathbf{x})$ is used to denote the mutual information between vectors $\hat{\mathbf{x}}$ and \mathbf{x} , and $\mathcal{H}(\hat{\mathbf{x}} | \mathbf{x})$ is the differential entropy of $\hat{\mathbf{x}}$ conditioned on \mathbf{x} .

IV. OPTIMIZATION PROBLEM

Putting together all the results presented in previous sections, the sum-rate maximization problem for C-RAN cluster c can

³The design of a RZF/MMSE precoder invariably requires of the noise variance experienced by the MSs, which needs somehow to be conveyed to the AP.

be formally expressed as

$$\begin{aligned} &\max_{\substack{\boldsymbol{\Upsilon}_c \geq 0 \\ \sigma_{q_c} \geq 0}} \sum_{m=1}^{N_{M_c}} \log_2 \left(1 + \frac{v_{c,m}}{\sum_{r=1}^{N_{Rc}} \sigma_{q_{c,r}}^2 \|\bar{\mathbf{h}}_{c,r,m}\|^2 + \sigma_n^2} \right) \\ &\text{s. t. } \left\| \overline{\mathbf{W}}_{c,r} \boldsymbol{\Upsilon}_c^{\frac{1}{2}} \right\|_F^2 + \sigma_{q_{c,r}}^2 \left\| \mathbf{W}_{c,r}^{(1)} \mathbf{W}_{c,r}^{(2)} \right\|_F^2 \leq \bar{P}_{c,r} \quad \forall r \in \mathcal{N}_{Rc} \\ &\quad \log_2 \det \left(\frac{\left\| \overline{\mathbf{W}}_{c,r} \boldsymbol{\Upsilon}_c^{\frac{1}{2}} \right\|_F^2}{\sigma_{q_{c,r}}^2} + \mathbf{I}_{r_{c,r}} \right) \leq \bar{C}_{c,r} \quad \forall r \in \mathcal{N}_{Rc}, \end{aligned} \quad (31)$$

where the precoding matrix of RRH r in cluster c (except for the power allocation matrix) is defined as $\overline{\mathbf{W}}_{c,r} = \mathbf{W}_{c,r}^{(1)} \mathbf{W}_{c,r}^{(2)} \overline{\mathbf{W}}_{c,r}^{(3)}$, and the vector characterizing the quantization noises in the fronthaul links between the c th CCU and the associated RRHs is $\boldsymbol{\sigma}_{q_c} = [\sigma_{q_{c,1}} \dots \sigma_{q_{c,N_{Rc}}}]^T$. Note that the first and second sets of restrictions in this optimization problem represent the transmit power constraints and the fronthaul rate constraints, respectively, for each of the RRHs in the cluster under evaluation.

For a fixed power allocation matrix $\boldsymbol{\Upsilon}_c$, the lower the quantization noise allowed on any of the N_{Rc} C-RAN fronthaul links, the higher the amount of quantized information that has to be transferred on these links. Furthermore, irrespective of the channel propagation conditions or the C-RAN FD-MIMO setup, the lower the quantization noise, the higher the amount of power available to transmit useful data and the higher the SINR experienced at the served MSs. Hence, it can be assert that the sum-rate in (31) is maximized when the fronthaul capacity constraints are satisfied with equality; that is, when

$$\det \left(\frac{\left\| \overline{\mathbf{W}}_{c,r} \boldsymbol{\Upsilon}_c^{\frac{1}{2}} \right\|_F^2}{\sigma_{q_{c,r}}^2} + \mathbf{I}_{r_{c,r}} \right) = 2^{\bar{C}_{c,r}} \quad \forall r \in \mathcal{N}_{Rc}. \quad (32)$$

The optimization problem in (31) can then be rewritten in terms of the power allocation matrix $\boldsymbol{\Upsilon}_c$ as in (33), as shown at the top of the next page, where $\sigma_{q_{c,r}}^2$ cannot be expressed as a closed-form algebraic expression and therefore only admits a solution in the form of a transcendental function $\sigma_{q_{c,r}}^2 = F(\boldsymbol{\Upsilon}_c, \overline{\mathbf{W}}_{c,r}^{(3)}, \bar{C}_{c,r})$ in terms of $\boldsymbol{\Upsilon}_c$ that can be numerically solved by applying mathematical software tools to (32).

A. SEEKING FOR A GLOBALLY OPTIMAL POWER ALLOCATION (GOPA)

As shown in Appendix, the transcendental function $\sigma_{q_{c,r}}^2 = F(\boldsymbol{\Upsilon}_c, \overline{\mathbf{W}}_{c,r}^{(3)}, \bar{C}_{c,r})$ is non-convex and thus, we are dealing with a challenging non-convex optimization problem. To tackle this challenge, we can resort to general purpose global optimization algorithms such as, for instance, the GlobalSearch or MultiStart schemes implemented in Matlab. In trying to find a global optimum solution, both

$$\begin{aligned} & \max_{\Upsilon_c \geq 0} \sum_{m=1}^{N_{Mc}} \log_2 \left(1 + \frac{\nu_{c,m}}{\sum_{r=1}^{N_{Rc}} F(\Upsilon_c, \bar{\mathbf{W}}_{c,r}^{(3)}, \bar{\mathbf{C}}_{c,r}) \|\bar{\mathbf{h}}_{c,r,m}\|^2 + \sigma_n^2} \right) \\ & \text{subject to } \left\| \bar{\mathbf{W}}_{c,r} \Upsilon_c^{1/2} \right\|_F^2 + F(\Upsilon_c, \bar{\mathbf{W}}_{c,r}^{(3)}, \bar{\mathbf{C}}_{c,r}) \left\| \mathbf{W}_{c,r}^{(1)} \mathbf{W}_{c,r}^{(2)} \right\|_F^2 \leq \bar{P}_{c,r} \quad \forall r \in \mathcal{N}_{Rc}, \end{aligned} \quad (33)$$

algorithms run a local solver under multiple starting points in order to explore a set of promising regions of attraction, defined as the set of starting points leading to the same local minimum (or maximum) when following the direction of steepest descend (or ascend). GlobalSearch uses a scatter-search mechanism to generate the set of starting points [37], whereas MultiStart uses uniformly distributed starting points located between user-provided upper and lower bounds. Needless to say, the high performance provided by these algorithms is always at the cost of a very high computational complexity that increases with the number of variables to optimize and the number of starting points being evaluated. It is not our aim in this work to explore the myriad of alternatives that could be found in the literature when implementing global optimization algorithms for this non-convex problem, our sole interest is to use one of the aforementioned general purpose global optimization algorithms to obtain a proper upper bound to benchmark the heuristic algorithm proposed in the following subsection.

B. HEURISTIC NORMALIZED OPTIMAL POWER ALLOCATION (NOPA)

The complexity of the GOPA approach when dealing with the optimization problem posed in (33) makes it slow, and therefore inefficient, particularly for those setups in which the number of MSs and/or RRHs per cluster are high. In order to speed up the process of finding a suboptimal yet satisfactory solution to this problem, a heuristic algorithm is proposed in this paper that is rooted on the vector normalization techniques used in massive MIMO precoding schemes with uniform power allocation (see, for instance, [28] and references therein), which will be termed as the NOPA strategy.

As it is stated in (8), RRH r in cluster c transmits a power $P_{Tc,r} \leq \bar{P}_{c,r}$ that can be split into two parts. The first one, that can be rewritten as

$$\text{tr} \left(\left\| \bar{\mathbf{W}}_{c,r} \Upsilon_c^{1/2} \right\|^2 \right) = \sum_{m=1}^{N_{Mc}} \nu_{c,m} \left\| \bar{\mathbf{w}}_{c,r,m} \right\|^2, \quad (34)$$

is the power dedicated to the transmission of useful information, and the second one,

$$\sigma_{q_{c,r}}^2 \left\| \mathbf{W}_{c,r}^{(1)} \mathbf{W}_{c,r}^{(2)} \right\|_F^2 = F(\Upsilon_c, \bar{\mathbf{W}}_{c,r}^{(3)}, \bar{\mathbf{C}}_{c,r}) \left\| \mathbf{W}_{c,r}^{(1)} \mathbf{W}_{c,r}^{(2)} \right\|_F^2, \quad (35)$$

is basically *wasted* power as it is effectively devoted to the transmission of quantization noise. Lim *et al.* [28] propose a vector normalized precoding scheme for a massive

MIMO system in the simple and practical case of uniform power allocation over all downlink transmitted streams.⁴ In the massive MIMO system considered by these authors, the CCU controls a group of RRHs that share a common total transmit power and, furthermore, infinite capacity fronthauls are considered and hence, quantization noise effects are neglected. In such a simplified scenario, there is only one power constraint per CCU that can be satisfied with equality by using (according to the mathematical notation introduced in our paper) $\nu_{c,m} = \left(\sum_{r'=1}^{N_{Rc}} \bar{P}_{c,r'} \right) / \left(N_{Mc} \left\| \bar{\mathbf{w}}_{c,m} \right\|^2 \right)$. Finite fronthaul capacity effects can be straightforwardly taken into account by introducing a multiplicative constant $0 < \beta_c \leq 1$ on the power allocation coefficients, that is, $\nu_{c,m} = \beta_c \left(\sum_{r'=1}^{N_{Rc}} \bar{P}_{c,r'} \right) / \left(N_{Mc} \left\| \bar{\mathbf{w}}_{c,m} \right\|^2 \right)$, to compensate for the *wasted* power dedicated to the transmission of quantization noise. In a more realistic C-RAN-based massive MIMO scenario, however, this power allocation strategy has to be reformulated to consider per-RRH power constraints. In order to ensure that the power allocation process satisfies the N_{Rc} power allocation constraints in (33), with at least one of the RRHs transmitting at maximum power, the normalization rule

$$\nu_{c,m} = \beta_c \xi_{c,m} = \beta_c \min_{r' \in \mathcal{N}_{Rc}} \left(\frac{\bar{P}_{c,r'}}{N_{Mc} \left\| \bar{\mathbf{w}}_{c,r',m} \right\|^2} \right), \quad (36)$$

is proposed in this paper, where β_c is obtained as

$$\beta_c = \left\{ x : \max_{r \in \mathcal{N}_{Rc}} \{ \varphi_{c,r}(x) + \alpha_{c,r}(x) - \bar{P}_{c,r} \} = 0 \right\}, \quad (37)$$

with

$$\varphi_{c,r}(x) = x \sum_{m=1}^{N_{Mc}} \xi_{c,m} \left\| \bar{\mathbf{w}}_{c,r,m} \right\|^2 \quad (38)$$

and

$$\alpha_{c,m}(x) = F \left(x \mathbf{\Xi}_c, \bar{\mathbf{W}}_{c,r}^{(3)}, \bar{\mathbf{C}}_{c,r} \right) \left\| \mathbf{W}_{c,r}^{(1)} \mathbf{W}_{c,r}^{(2)} \right\|_F^2, \quad (39)$$

using $\mathbf{\Xi}_c = \text{diag}(\xi_{c,1}, \dots, \xi_{c,N_{Rc}})$. Although this is a sub-optimal heuristic algorithm, numerical results presented in Section V clearly show that the NOPA approach suffers from minor performance losses when compared to the GOPA solution at an affordable computational complexity.

⁴As stated by Lim *et al.* [28], in massive MIMO systems using uniform power allocation over all downlink transmitted streams there is an alternative to the vector normalization that is termed as matrix normalization. This strategy, however, cannot be implemented in distributed massive MIMO scenarios like those found in the context of C-RAN.

C. BENCHMARKING SYSTEM: MULTI-LAYER FD MASSIVE MIMO

The multi-layer FD massive MIMO system [21] has a single BS per cell and thus, in contrast to the proposed C-RAN scenario, it does not use neither clusterization nor fronthauling between the BS and a CCU. The analytical model for this benchmarking system can be interpreted as a particular case of the one previously developed for the C-RAN scheme where $N_{Rc} = 1$ (no clusterization) and $\bar{C}_{c,1} = \infty$ (no fronthauling). In this case, problem (33) simplifies to

$$\begin{aligned} & \max_{\mathbf{v}_c \geq 0} \sum_{m=1}^{N_{Mc}} \log_2 \left(1 + \frac{v_{c,m}}{\sigma_n^2} \right) \\ & \text{subject to } \sum_{m=1}^{N_{Mc}} \|\bar{\mathbf{w}}_{c,1,m}\|^2 v_{c,m} \leq \bar{P}_{c,1}, \end{aligned} \quad (40)$$

which has a closed form that can be easily found by waterfilling as

$$v_{c,m} = \max \left\{ 0, \frac{1}{\mu_c \|\bar{\mathbf{w}}_{c,1,m}\|^2 \ln 2} - \sigma_n^2 \right\} \quad (41)$$

where the water level μ_c is chosen to satisfy the constraint in (40) with equality. Even though we are not implementing any global optimization algorithm as those used to solve the multi-layer C-RAN FD massive MIMO case, with a slight abuse of notation, the waterfilling-based approach will also be denoted as the GOPA solution. Just like the C-RAN strategy, the multi-layer FD massive MIMO system also admits a simpler heuristic closed-form NOPA solution that can be expressed as

$$v_{c,m} = \frac{\bar{P}_{c,1}}{N_{Mc} \|\bar{\mathbf{w}}_{c,1,m}\|^2}. \quad (42)$$

V. NUMERICAL RESULTS

Simulation results are presented in this section that serve to demonstrate the performance of the multi-layer downlink precoding for C-RAN systems using FD massive MIMO proposed in previous sections. For simplicity of exposition, the downlink of a C-RAN is considered where all RRHs are located on an upright square lattice and $N_C = 9$ squared mutually interfering clusters are formed [11], each consisting of $N_{Rc} = 4, 9$ or 16 RRHs controlled by a single CCU. A random snapshot of such a network topology with $N_{Rc} = 9$ RRHs/cluster (square markers) and $N_{Mc} = 20$ uniformly distributed MSs/cluster (circle markers) is depicted in Fig. 3. The inter-cluster distance (i.e., the distance between the centers of neighboring squared clusters or, equivalently, the side of the square representing a cluster) has been denoted by D . Furthermore, although in the simulations the boundaries between clusters will be blurred by the effects of shadow fading, solid lines have been used to schematically represent the cluster coverage areas.

The channel propagation losses between RRH r in cluster c' and MS m in cluster c have been modeled

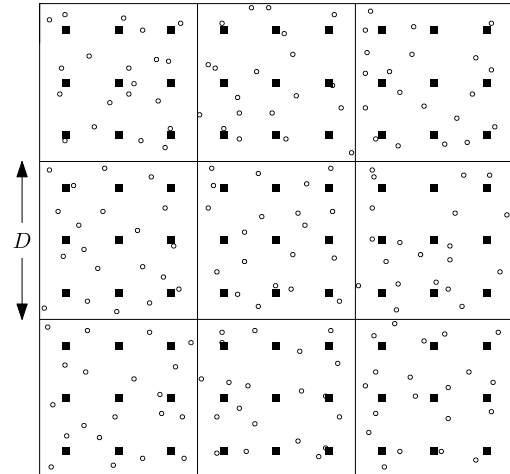


FIGURE 3. A realization of a C-RAN with $N_C = 9$ clusters, $N_{Rc} = 9$ RRHs/cluster (square markers) and $N_{Mc} = 20$ MSs/cluster (circle markers).

as [38]

$$\begin{aligned} \text{PL}_{c,m}^{c',r} = & (44.9 - 6.55 \log_{10}(h_{c',r})) \log_{10}(d_{c,m}^{c',r}) + 34.46 \\ & + 5.83 \log_{10}(h_{c',r}) + 23 \log_{10}(f_0/5.0) \\ & - G_{Rc,m} - G_{Tc',r} \left(\theta_{c,m}^{c',r} \right) + X_{c,m}^{c',r}, \end{aligned}$$

where $h_{c',r}$ is the antenna height (in meters) of the r th RRH in cluster c' , $d_{c,m}^{c',r}$ is the distance (in m) between MS m in cluster c and RRH r in cluster c' , f_0 is the carrier frequency (in GHz), $G_{Rc,m}$ is the receive antenna gain (in dB) of MS m in cluster c , $G_{Tc',r} \left(\theta_{c,m}^{c',r} \right)$ is the transmit antenna gain (in dB) of RRH r in cluster c' in the direction of the elevation angle $\theta_{c,m}^{c',r}$ of MS m in cluster c , which can be expressed as

$$G_{Tc',r} \left(\theta_{c,m}^{c',r} \right) = G_{Tc',r}^{\text{MAX}} - \min \left(12 \left(\frac{\theta_{c,m}^{c',r} - \theta_{c',r}^{\text{tilt}}}{\theta_{c',r}^{3dB}} \right)^2, A_{c',r}^{\text{BL}} \right),$$

with $G_{Tc',r}^{\text{MAX}}$, $\theta_{c',r}^{\text{tilt}}$, $\theta_{c',r}^{3dB}$ and $A_{c',r}^{\text{BL}}$ denoting, respectively, the boresight gain, the (electrical) downtilt, the 3dB-beamwidth and the back-lobe attenuation of this antenna, and finally, $X_{c,m}^{c',r} \sim \mathcal{N}(0, \sigma_s^2)$ is the shadow fading (in dB) experienced on this link. As shadowing effects caused by obstacles in the propagation path between the RRH and the MS affect large areas in the vicinity of a given MS, a two-dimensional Gaussian process with appropriate spatial correlation is typically used to capture the dynamics affecting the shadowing experienced by either a given MS when receiving information from different RRHs or different neighboring MSs when receiving information from a given RRH. In this work, a low-complexity method has been used to introduce both spatial and inter-site correlation into the Gaussian process while preserving its statistical properties (see [39] for details).

Assuming that the RRHs are elevated away from nearby obstacles and that the MSs are surrounded by local scatterers, Kronecker product-based approximations for the spatial

correlation of different antenna topologies for FD massive MIMO systems can be derived (see, for instance, [17], [18]). The URA spatial correlation approximation proposed by Ying *et al.* [17] has been considered in this work, notwithstanding that the proposed analytical framework could be readily extended to incorporate other Kronecker product-based approximations or other FD massive MIMO antenna topologies, such as the cylindrical array [18]. Using this model, the correlation between the signals radiated by any pair of antenna elements of the (c', r) th URA in the vertical (elevation) and horizontal (azimuth) directions can be obtained using [17, eqs. (25) and (25)], respectively, where we have assumed the elevation and azimuth angular perturbations experienced by MS m in cluster c to be statistically distributed as $\mathcal{N}(0, \xi_{c,m}^{c',r})$ and $\mathcal{N}(0, \sigma_{c,m}^{c',r})$, respectively. The elevation and azimuth angular standard deviations have been approximated as $\xi_{c,m}^{c',r} = \arctan(\Delta_{c,m}^E / d_{c,m}^{c',r})$ and $\sigma_{c,m}^{c',r} = \arctan(\Delta_{c,m}^A / d_{c,m}^{c',r})$, respectively, where $\Delta_{c,m}^E$ and $\Delta_{c,m}^A$ are used to denote the standard deviation of the distance spread between the MS and the surrounding scatterers in both the elevation and azimuth directions.

The performance analysis presented in the upcoming subsections is based on the following metrics:

- **Spectral efficiency:** Defined as the sum-rate (measured in bit/s/Hz) the N_{Rc} cooperating RRHs in cluster c offer to the set of N_{Mc} scheduled MSs.
- **Coverage probability:** Defined as the probability that the instantaneous rate the N_{Rc} cooperating RRHs in cluster c provide to a generic MS is higher than a given threshold.

Default parameters used to set-up the simulation scenarios under evaluation in the following subsections are summarized in Table 1. Furthermore, for the sake of accuracy, each simulation has been executed over 100 transmission time intervals (i.e., channel uses) and repeated for 1000 different random locations of the MSs.

A. MODIFYING THE NUMBER OF RRHs PER CLUSTER

Our aim in this subsection is to analyze how increasing the number of RRHs per cluster affects the performance of the proposed multi-layer downlink precoding approach. Results for the C-RAN system will be benchmarked against the performance provided by an *equivalent* massive MIMO arrangement. In order to achieve the same number of spatial DoFs per MS as well as *equivalent* system configurations, the total number of transmit antennas per cluster (i.e., $\sum_{r=1}^{N_{Rc}} n_{Tc,r}^A n_{Tc,r}^E$) and the available transmit power per cluster (i.e., $\sum_{r=1}^{N_{Rc}} P_{Tc,r}$) will be the same for all scenarios under comparison. Furthermore, taking into account that as the number of RRHs per cluster increases and the transmit power decreases, the area of influence of each RRH shrinks and the height to which the FD massive MIMO antennas are installed is typically lower, it has been assumed in this work that, given a reference antenna height h , all the RRHs have a

TABLE 1. Summary of default simulation parameters.

Parameters	Value
Number of clusters: N_C	9
Number of RRHs/cluster: N_{Rc}	9
Number of MSs/cluster: N_{Mc}	15
Transmit power per cluster: P_{Tc}	47 dBm
RRH antenna radiation pattern [16]: $G_{Tc,r}^{\text{MAX}}$	17 dBi
$\theta_{c,r}^{\text{tilt}}$	$-\pi/30$ rad
$\theta_{c,r}^{3dB}$	$3\pi/8$ rad
$A_{c,r}^{\text{BL}}$	30 dB
MS antenna gain: $G_{Rc,m}$	3 dBi
MS noise figure: NF_{MS}	7 dB
Background noise: N_0	-174 dBm/Hz
Distance between neighboring clusters: D	500 m
Shadowing standard deviation: σ_s	8 dB
Shadowing decorrelation distance: d_d	20 m
Shadowing correlation factor among RRHs	0.5
Carrier frequency: f_0	4 GHz
Reference height of the RRHs: h	60 m
Height of the MSs: $h_{c,m}$	1.5 m
Distance among neighboring elements in the URA: d	$\lambda/2$
Azimuth distance standard deviation: $\Delta_{c,m}^A$	1.5 m
Elevation distance standard deviation: $\Delta_{c,m}^E$	0.9 m

massive MIMO array installed at a height $h_{c',r} = h/\sqrt{N_{Rc'}}$ (note that for a fixed cluster side D , the distance between RRHs is also given by $D/\sqrt{N_{Rc'}}$).⁵ As for the fronthaul capacity, two different configurations will be considered. In the first configuration it will be assumed that a fixed fronthaul capacity per cluster is equally split among the corresponding RRHs. In the second configuration, instead, it will be assumed that the fronthaul capacity per CCU-RRH link is kept fixed irrespective of the number of RRHs/cluster.

In Fig. 4 we compare the spectral efficiency per cluster, the average power factor per symbol and the average variance of the quantization noise provided by different set-ups of the proposed C-RAN approach. All the performance results are represented as a function of the fronthaul capacity per cluster and the spectral efficiency is benchmarked against that provided by a massive MIMO system. In order to make all the set-ups *equivalent*, the number of vertical antenna elements in the URAs has been fixed to $n_{Tc,r}^E = 96$, and the number of horizontal antenna elements has been set to $n_{Tc,r}^A = 32$ for the massive MIMO configuration and to $n_{Tc,r}^A = 8$ and 9 for the C-RAN scenarios with $N_{Rc} = 4$ and 16 , respectively. For the C-RAN scenarios with $N_{Rc} = 9$, five of the RRHs have been randomly selected and have been allocated $n_{Tc,r}^A = 4$ antenna elements and the rest of RRHs have been allocated $n_{Tc,r}^A = 3$ antenna elements. The first important result to note from Fig. 4a is that the NOPA approach provides spectral efficiencies that are only slightly inferior to those provided by the GOPA strategy, even though the latter is considerably

⁵The proposed framework is general enough so as to cater for non-regular locations of the RRHs, for random distributions of the transmit antenna heights, for different radiation diagrams and/or for other massive MIMO antenna topologies, but the evaluation of such a myriad of possibilities is far beyond the scope of this work.

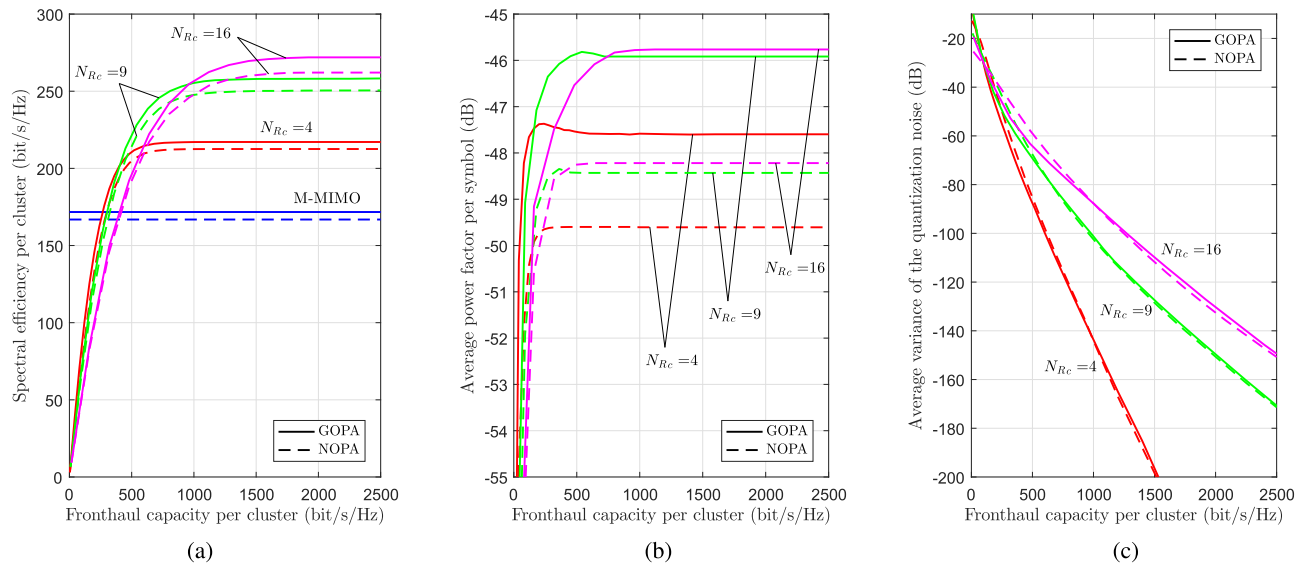


FIGURE 4. The spectral efficiency per cluster, average power factor per symbol and average quantization noise variance provided by the proposed C-RAN approach are compared to those provided by an equivalent massive MIMO system, all of them using URAs with $n_{Tc,r}^E = 96$ vertical antenna elements. The number of horizontal antenna elements has been set to $n_{Tc,r}^A = 32$ for the massive MIMO configuration and to $n_{Tc,r}^A = 8, 4$ (or 3), or 2 for the C-RAN scenarios with $N_{Rc} = 4, 9$ or 16, respectively. (a) Spectral efficiency per cluster. (b) Average power factor per symbol. (c) Average quantization noise variance.

more complex than the former. Hence, in C-RAN scenarios where complexity is an issue, the NOPA-based frameworks constitute a very good alternative to GOPA-based systems. As expected, in scenarios with a very low aggregate fronthaul capacity per cluster, the precoded information that has to be transferred from the CCU to the RRHs has to be quantified with a very high quantization noise (see Fig. 4c). In this case, as shown in Fig. 4b, a large portion of the available transmit power is literally wasted by both the GOPA and the NOPA schemes in the process of transmitting the quantization noise. A direct consequence of the combined effects of a reduced *useful* transmit power and an increased quantization noise is a very poor spectral efficiency (see Fig. 4a) that, depending on the specific value of $\bar{C}_{c,r}$, can even be lower than that provided by the *equivalent* massive MIMO scheme. For the particular set-ups under consideration, the spectral efficiency values provided by the massive MIMO scheme using either GOPA or NOPA is equal to 171.7 bit/s/Hz and 166.9 bit/s/Hz, respectively, and these are only overcome by those provided by an *equivalent* FD massive MIMO-based C-RAN system with $N_{Rc} = 4, 9$ or 16 RRHs/cluster when $\bar{C}_{c,r} \geq 267.8, 303.1$ or 403 bit/s/Hz, for the GOPA case, respectively, and when $\bar{C}_{c,r} \geq 284, 310.5$ or 398.7 bit/s/Hz, respectively, for the NOPA case. As the fronthaul capacity per cluster increases beyond these values, the spectral efficiency gain provided by the C-RAN schemes when compared to that provided by the massive MIMO approach rises until reaching a saturation value. It is worth noting that, the convenience of using one or another setup will basically depend on the available fronthaul capacity per cluster, the power allocation strategy under use and the implementation complexity that

can be afforded. In general, as shown in Fig. 4a, the higher the fronthaul capacity per cluster the higher is the number of RRHs/cluster that have to be installed to maximize the spectral efficiency. Anyway, a C-RAN set-up with $N_{Rc} = 9$ RRHs/cluster seems to provide most of the spectral efficiency gain that these systems can offer when compared to the massive MIMO setup.

Instead of assuming a fixed fronthaul capacity per cluster equally split among the corresponding RRHs, the proposed multi-layer precoding-based C-RAN with FD massive MIMO can also be evaluated under the assumption of a fixed fronthaul capacity per CCU-RRH link irrespective of the number of RRHs/cluster. Results obtained assuming these particular conditions are presented in Fig. 5 under different FD massive MIMO antenna configurations. To obtain results presented in Fig. 5a, URAs with a fixed number of vertical elements and a variable number of horizontal antennas have been considered. In particular, the number of vertical antenna elements has been fixed to $n_{Tc,r}^E = 96$ and the number of horizontal antenna elements has been set to $n_{Tc,r}^A = 32$ for the massive MIMO configuration and to $n_{Tc,r}^A = 8, 4$ (or 3), and 2 for the C-RAN scenarios with $N_{Rc} = 4, 9$ or 16, respectively. Again, similar to the effects observed in Fig. 4a (in essence, there has only been a change of scale), the *equivalent* massive MIMO scheme provides higher spectral efficiencies than C-RAN-based schemes for very low values of the fronthaul capacity per CCU-RRH link, and as this fronthaul capacity increases the spectral efficiency provided by the C-RAN-based systems eventually surpasses that provided by the massive MIMO scheme until reaching a saturation value. Fixing the fronthaul capacity per CCU-RRH link

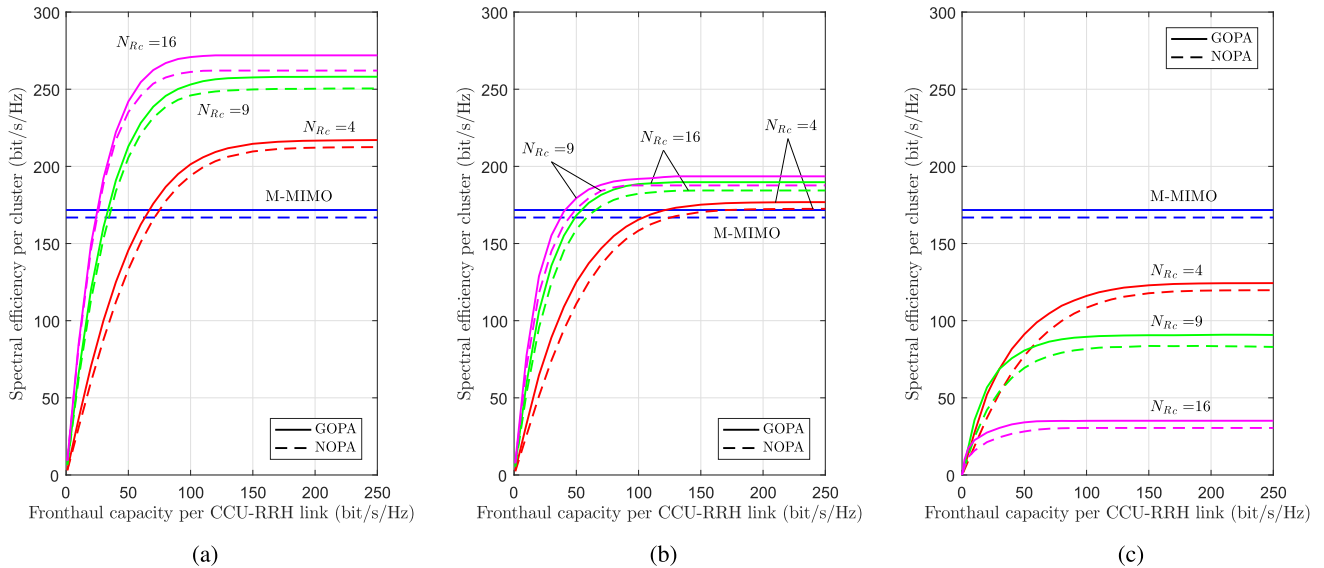
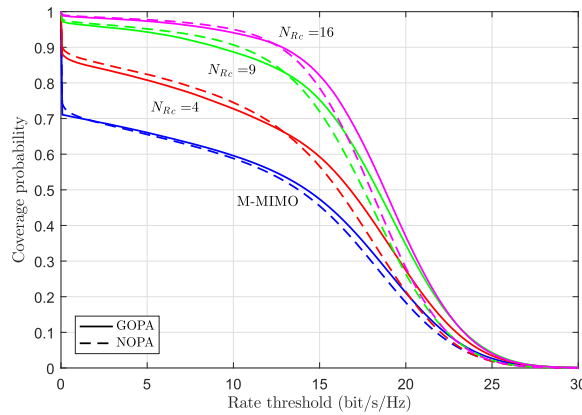


FIGURE 5. The spectral efficiency per cluster provided by the proposed multi-layer precoding-based C-RAN with FD massive MIMO under different antenna configurations is compared to that provided by an equivalent massive MIMO system. All the configurations assume the use of $N_R n_{T_{C,r}}^A n_{T_{C,r}}^E = 3072$ antenna elements. (a) SE/cluster - $n_{T_{C,r}}^E = 96$. (b) SE/cluster - $n_{T_{C,r}}^A / n_{T_{C,r}}^E = 1/3$. (c) SE/cluster - $n_{T_{C,r}}^A = 32$.

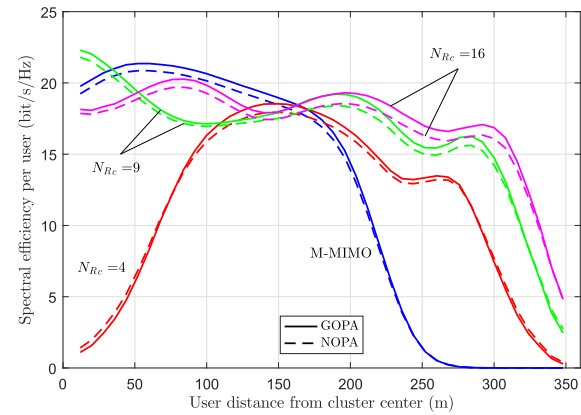
confers a non-negligible performance advantage to C-RAN-based schemes as the number of RRHs per cluster increases, although it can again be observed that $N_{Rc} = 9$ seems to lead to an attractive operational setup. Results presented in Fig. 5b correspond to an FD massive MIMO antenna configuration in which both the total number of antenna elements per cluster and the ratio between vertical and horizontal antenna elements are kept constant. The FD massive MIMO setup is exactly the same that has been used to obtain the results in Fig. 5a. In the C-RAN scenarios, however, the number of vertical and horizontal antenna elements have been set to $n_{T_{C,r}}^E = 48, 32$ and 24 and $n_{T_{C,r}}^A = 16, 11/10$ (six RRHs with 11 antenna elements and 3 RRHs with only 10 antenna elements), or 8 for the C-RAN scenarios with $N_{Rc} = 4, 9$ or 16 , respectively. Results presented in Fig. 5c, however, correspond to an FD massive MIMO antenna configuration where the number of horizontal antenna elements has been fixed to $n_{T_{C,r}}^A = 32$ and the number of vertical antenna elements has been set to $n_{T_{C,r}}^E = 96$ for the massive MIMO configuration and to $n_{T_{C,r}}^E = 24, 11/10$, or 6 for the C-RAN scenarios with $N_{Rc} = 4, 9$ or 16 , respectively. The main conclusion that can be drawn from the performance comparison of all *equivalent* configurations considered in Figs. 5a-5c is that a multi-layer precoding-based FD massive MIMO scheme requires of a large number of vertical antenna elements to provide a proper inter-cluster interference cancellation without sacrificing intra-cluster service coverage. Consequently, decreasing the number of vertical antenna elements, as it has been done in the configurations analyzed in Figs. 5b and 5c, eventually translates into a high spectral efficiency loss. Particularly remarkable is the performance loss experienced by the C-RAN configurations with a fixed number of horizontal antennas, as shown in 5c. This performance loss is basically

due to the decrease of spatial DoFs the first precoding layer causes when cancelling inter-cluster interference that greatly complicates implementing the subsequent ZF precoding scheme to get rid of the intra-cluster interference.

Assuming that the total number of antenna elements in a cluster is kept constant, it has been just shown that one of the best FD massive MIMO antenna configurations consists of using a large enough number of vertical antenna elements and adjusting the number of horizontal elements according to the number of RRHs/cluster. To gain further insight into this particular antenna configuration, let us determine the rate coverage probability and the spectral efficiency experienced by a particular MS as a function of its distance from the center of the cluster. Again, the number of vertical antenna elements in the URAs is fixed to $n_{T_{c,r}}^E = 96$, and the number of horizontal antenna elements is set to $n_{T_{c,r}}^A = 32$ for the massive MIMO configuration and to $n_{T_{c,r}}^A = 8, 4/3$, or 2 for the C-RAN scenarios with $N_{Rc} = 4, 9$ or 16, respectively. The rate coverage probability is plotted in Fig. 6a. Results show that, increasing the number of RRHs per cluster is always beneficial from the coverage probability point of view, with the C-RAN-based approach clearly outperforming the benchmarking massive MIMO scheme. Results also show that when implementing a multi-layer precoding-based FD massive MIMO scheme there is a high probability (circa 0.3) that there are some MSs suffering from severe blockage. The blockage probability is still quite high (circa 0.12) for the C-RAN-based scheme with $N_{Rc} = 4$ RRHs/cluster and it becomes almost negligible for C-RAN-based scenarios with $N_{Rc} = 9$ or 16 RRHs/cluster. The first-layer precoding process is designed with the aim of removing the out-of-cluster interference or, equivalently, it is designed to avoid the transmission of information to MSs in other clusters, whose elevation angles with respect

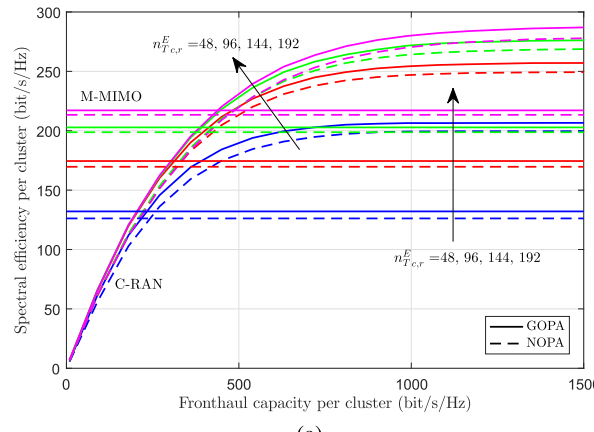


(a)

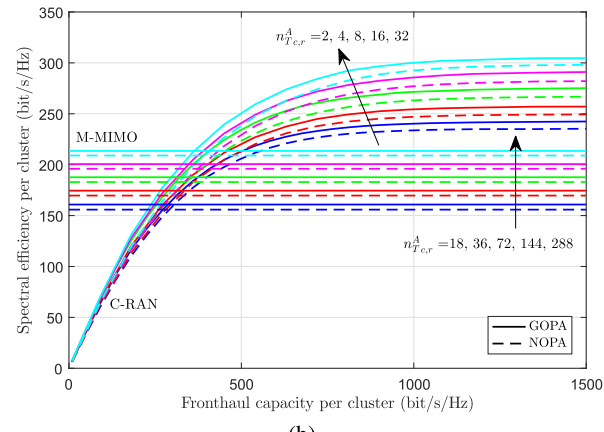


(b)

FIGURE 6. Coverage probability and spectral efficiency per MS versus distance from the cluster center (URAs with $n_{T_{C,r}}^E = 96$ and $n_{T_{C,r}}^A = 32$ antenna elements for the M-MIMO configuration and $n_{T_{C,r}}^A = 8, 4/3$, or 2 for the C-RAN scenarios with $N_{Rc} = 4, 9$ or 16, respectively). (a) Coverage probability. (b) SE/MS vs distance from cluster center.



(a)



(b)

FIGURE 7. The spectral efficiency per cluster provided by the proposed C-RAN approach with $N_{Rc} = 9$ RRHs/cluster is compared to that provided by an equivalent massive MIMO scheme under different FD massive MIMO antenna configurations. (a) SE/cluster vs $n_{T_{C,r}}^E$ ($n_{T_{C,r}}^A = 36/4$ for M-MIMO/C-RAN). (b) SE/cluster vs SE/cluster vs $n_{T_{C,r}}^A$ ($n_{T_{C,r}}^E = 96$ for M-MIMO and C-RAN).

to a given RRH are typically higher than those characterizing the MSs in the cluster of interest. The problem is that there can be MSs in the cluster of interest whose elevation angle is similar to those characterizing some of the MSs in other clusters and thus, they will also suffer from critical blockage. As shown in Fig. 6b, which represents the spectral efficiency per MS as a function of its distance from the cluster center, the group of MSs experiencing blockage is quite different for the various scenarios under consideration. In scenarios based on the benchmarking FD massive MIMO scheme the *blocked* MSs are located in a quite wide region near the cluster edge (MSs located beyond ~ 270 meters from the center of the cluster). The C-RAN-based scenario with $N_{Rc} = 4$ RRHs/cluster shows a particular geometric configuration that produces the blockage, not only of the MSs that are very close to the cluster edge, but also of those that occupy the center of the cluster. This is basically due to that both groups of MSs share similar elevation angles as observed from any of the RRHs constituting the cluster of interest and thus, the

elevation correlation matrices of MSs in the center of the cluster are also in the null space of those of MSs located in interfering clusters (therefore, geometric configurations with $N_{Rc} = 4$ RRHs/cluster should be avoided). The spectral efficiency of MSs located near the cluster edge in C-RAN-based scenarios with $N_{Rc} = 9$ and 16 RRHs/cluster is seriously affected by the first-layer precoding process but these MSs only very sporadically suffer from blockage. Thus, using C-RAN-based strategies with $N_{Rc} = 9$ or 16 RRHs/cluster significantly improves the spectral efficiency fairness among MSs.

B. MODIFYING THE NUMBER OF ANTENNA ELEMENTS

To better understand how the number of antenna elements in the URAs influence the performance of the proposed C-RAN-based scheme, Fig. 7 compares the spectral efficiency per cluster provided by the C-RAN approach assuming the use of $N_{Rc} = 9$ RRHs/cluster to that provided by an

equivalent massive MIMO scheme under different FD massive MIMO antenna configurations. Figure 7a shows the spectral efficiency per cluster versus the fronthaul capacity per cluster with the number of vertical antenna elements of the URAs as parameter. The number of horizontal antenna elements has been set to $n_{T_{c,r}}^A = 36$ and 4 for the massive MIMO and C-RAN scenarios, respectively. Consistently with results presented in the previous subsection, using a low number of vertical antenna elements results in a significant sacrifice of spectral efficiency. The intuition behind this result lies in the reduction of DoFs caused when designing the first-layer precoding for intercluster interference avoidance. As the number of vertical antenna elements increases, the system can transmit on the null space of the interfering clusters while still leaving room for a proper implementation of the intra-cluster multi-user interference cancellation through the use of the ZF precoders. Observe that the increase in spectral efficiency performance is subject to the law of diminishing returns as the number of vertical antenna elements is incrementally increased and hence, in this particular scenario, using URA configurations with more than 140-150 vertical antenna elements would not be highly recommended. Another interesting result is that, even though the spectral efficiency gains seem to decrease with the number of vertical antenna elements, the proposed C-RAN provides a clear performance advantage over the benchmarking massive MIMO scheme. As shown in Fig. 7b, spectral efficiency performance gains can also be obtained by increasing the number of horizontal antenna elements and, in fact, the performance gains of the C-RAN approach when compared to the massive MIMO system do not seem to suffer from the law of diminishing returns, effects so clearly observed when increasing the number of vertical antenna elements. Furthermore, note that irrespective of the antenna configuration the low-complexity NOPA strategy provides spectral efficiencies that are only slightly inferior to those provided by the much more complex GOPA arrangement.

C. IMPACT OF THE NUMBER OF MSs PER CLUSTER

As shown in Fig. 8, the spectral efficiency increases with the number of active MSs per cluster for both the *benchmarking* massive MIMO setup and the proposed C-RAN scheme, and irrespective of the power allocation strategy under use. Results presented in this figure have been obtained assuming a massive MIMO BS equipped with $n_{T_{c,r}}^E = 96$ and $n_{T_{c,r}}^A = 32$ vertical and horizontal antenna elements, respectively, and a set of $N_{R_c} = 9$ RRHs/cluster equipped with fronthaul links with a capacity of $\bar{C}_{c,r} = 50, 100$ or 150 bit/s/Hz and configuring an *equivalent* C-RAN-based scheme with $n_{T_{c,r}}^E = 96$ vertical antenna elements and $n_{T_{c,r}}^A = 4$ or 3 (five and four RRHs with four and three horizontal antenna elements, respectively). Note that the GOPA and NOPA algorithms provide almost the same spectral efficiency in scenarios in which there are few MSs per cluster and that the performance differences, although not very remarkable, become more and

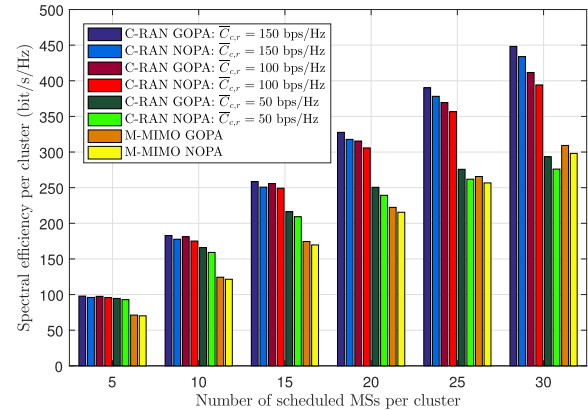


FIGURE 8. Spectral efficiency per cluster versus the number of MSs per cluster (C-RAN: $N_{R_c} = 9$, $n_{T_{c,r}}^E = 96$, $n_{T_{c,r}}^A = 4$ or 3. Equivalent massive MIMO: $n_{T_{c,r}}^E = 96$ and $n_{T_{c,r}}^A = 32$).

more evident as the number of MSs per cluster increases. Regardless of the technique in use, the increase of spectral efficiency does not linearly grow with an increasing number of MSs/cluster but, as can be hinted from the results presented in Fig. 8, it tends to saturate. This saturation is basically due to two distinct effects. Firstly, the well-known multiuser diversity provided by wireless fading channels saturates as the number of MSs/cluster increases. Secondly, and specific to the case of C-RAN, the more MSs in the system the more resources are consumed at the fronthaul and thus, as results in Fig. 8 clearly show, increasing the number of MSs in the system when the fronthaul resources are not adequately expanded causes the C-RAN architecture performance to saturate at a faster pace than that of the massive MIMO scheme (i.e., the lower the fronthaul capacity per cluster, the faster the saturation pace becomes). In fact, under extremely stringent fronthaul capacity constraints, the performance of the C-RAN-based architecture can fall even below that achieved by the M-MIMO-based configuration (see, for instance, results obtained for a 50 bps/Hz fronthaul and 30 MSs/cluster). That is, the performance advantages of the proposed C-RAN scheme when compared with the *benchmarking* massive MIMO arrangement can only be guaranteed if the capacity of the fronthaul links increases in parallel with the increase in the number of MSs per cluster.

D. IMPACT OF ANTENNA HEIGHTS AND CLUSTER COVERAGE AREA

The impact the RRH antenna height and the cluster coverage area may have on the achievable spectral efficiency is evaluated in Fig. 9. Results have been obtained adopting the same antenna and fronthaul configurations as in the previous subsection. The proposed C-RAN approach clearly outperforms the *benchmarking* massive MIMO scheme irrespective of the network characteristics under evaluation. As shown in Fig. 9a, increasing the cluster side leads to a decrease in the spectral efficiency per cluster that, even though it can also be influenced by the variation of the pointing elevation

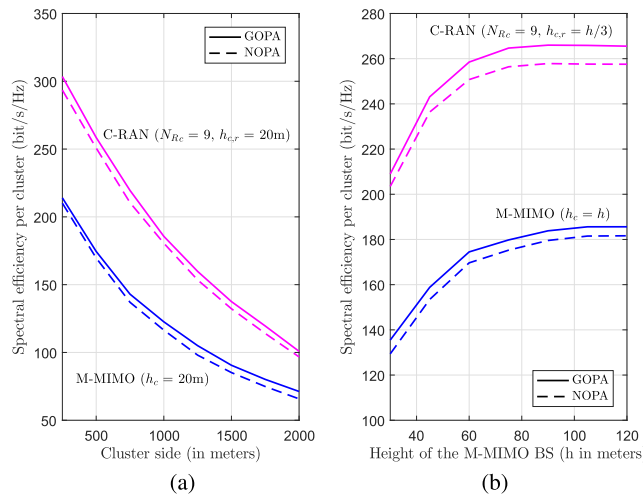


FIGURE 9. Spectral efficiency per cluster versus cluster side and antenna height (C-RAN: $N_{Re} = 9$, $n_{Tc,r}^E = 96$, $n_{Tc,r}^A = 4$ or 3, $\bar{C}_{c,r} = 150$ bit/s/Hz. Equivalent massive MIMO: $n_{Tc,r}^E = 96$ and $n_{Tc,r}^A = 32$). (a) SE/cluster vs cluster side. (b) SE/cluster vs antenna height.

angles to the interfering clusters, it is basically due to the increased path loss attenuation values. The effects the variation of the null space configuration of the interfering clusters may have on the performance of both the proposed C-RAN approach and the *equivalent* massive MIMO system are much more evidenced by the modification of the antenna height. Using low antenna heights degrades the spectral efficiency performance of both transmission strategies because forcing the transmission in the elevation null space of the interfering clusters under these conditions has a very strong impact on the blockage suffered by MSs located near the cluster edge. This is because these MSs are located at elevation angles that are very similar to those characterizing the MSs located in interfering clusters. The difference between these elevation angles increases with the antenna height and this seems to benefit the spectral efficiency per cluster as can be observed in Fig. 9b.

VI. CONCLUSION

A novel framework for low-complexity multi-layer downlink precoding in multi-cluster C-RAN systems using FD massive MIMO has been presented in this paper. The proposed approach leverages the large time-scale statistics of the 3D MIMO channels characterizing the propagation between the RRHs in a cluster and the served MSs to efficiently manage both the C-RAN-related inter- and intra-cluster interference and the pilot contamination associated to the channel estimation process in massive MIMO systems. The proposed multi-layer approach has been successfully adapted to the CAP-based CCU-RRH functional split, achieving full RRH cooperation with low implementation complexity and low CSI requirements. Optimal and suboptimal solutions, termed as GOPA and NOPA, respectively, have been provided than take into account both the per-RRH transmit power constraints and the capacity constraints of the fronthaul links

between the CCU and the associated RRHs. Grounded on the vector normalization techniques used in massive MIMO, the suboptimal approach has been shown to suffer from minor spectral efficiency losses when compared to the far more complex optimal solution. Furthermore, results have evidenced that, assuming the use of high-capacity fronthaul links, the proposed C-RAN-based approach achieves clear spectral efficiency gains with respect to the *classical* non-cooperative multi-cell FD massive MIMO scheme. Moreover, as the number of RRHs per cluster increases, the proposed C-RAN-based strategy increases the spectral efficiency fairness among users across the cluster. In the simulation scenarios considered in this paper, a C-RAN set-up with only 9 RRHs/cluster has been shown to provide most of the spectral efficiency and fairness gains that these systems can offer when compared to the *benchmarking* massive MIMO system. Another interesting conclusion is that, irrespective of the system under consideration, a multi-layer precoding-based FD massive MIMO scheme requires of a large enough number of vertical antenna elements (somewhere between 80 and 140 antenna elements) to provide a proper inter-cluster interference cancellation without sacrificing intra-cluster service coverage. For future work, it would be interesting to investigate both the spectral and energy efficiencies of this approach when implemented in multi-tier heterogeneous C-RANs, when using other CCU-RRH functional splits and/or when implemented using hybrid analog/digital architectures in mmWave massive MIMO systems.

APPENDIX

ON THE NON-CONVEXITY OF $\sigma_{q_{c,r}}^2 = \mathbf{F}(\Upsilon_c, \bar{\mathbf{W}}_{c,r}^{(3)}, \bar{\mathbf{C}}_{c,r})$

A continuous, twice differentiable function of several variables is convex on a convex set if and only if its Hessian matrix of second partial derivatives is positive semi-definite on the interior of the convex set. Thus, an easy way to demonstrate that $\sigma_{q_{c,r}}^2$ is non-convex is by proving that at least one of the diagonal components of the Hessian matrix is negative.

In matrix theory, the Sylvester's determinant identity states that if \mathbf{A} and \mathbf{B} are rectangular matrices of size $m \times n$ and $n \times m$, respectively, then $\det(\mathbf{I}_m + \mathbf{AB}) = \det(\mathbf{I}_n + \mathbf{BA})$, hence, (32) can be rewritten as

$$\det\left(\Phi_{c,r}\Upsilon_c/\sigma_{q_{c,r}}^2 + \mathbf{I}_{N_{Mc}}\right) = 2^{\bar{C}_{c,r}} \quad \forall r \in \mathcal{N}_{Rc}, \quad (43)$$

where $\Phi_{c,r} \triangleq \bar{\mathbf{W}}_{c,r}^{(3)H} \bar{\mathbf{W}}_{c,r}^{(3)}$ is an $N_{Mc} \times N_{Mc}$ Hermitian positive semi-definite matrix that can be diagonalized as $\Phi_{c,r} = \mathbf{V}_{c,r} \boldsymbol{\Omega}_{c,r} \mathbf{V}_{c,r}^H$, with $\boldsymbol{\Omega}_{c,r} = \text{diag}(\omega_{c,r,1}, \dots, \omega_{c,r,N_{Mc}})$. Furthermore, as $\Phi_{c,r}$ and Υ_c commute, they can be simultaneously diagonalized and thus, the eigenvalues of $\Phi_{c,r}\Upsilon_c$ are products of the eigenvalues of $\Phi_{c,r}$ and the diagonal elements of Υ_c . Using this property, (43) can be rewritten in terms of the eigenvalues of $\Phi_{c,r}$ and the diagonal elements of Υ_c as

$$\prod_{m=1}^{N_{Mc}} \left(\omega_{\pi_{c,r}(m)} x_m / \sigma_{q_{c,r}}^2 + 1 \right) = 2^{\bar{C}_{c,r}} \quad \forall r \in \mathcal{N}_{Rc}, \quad (44)$$

where $\pi_{c,r}(m)$ represents a particular permutation of subindex m . Implicitly differentiating (44) with respect to x_m , the first partial derivative of $\sigma_{q_{c,r}}^2$ can be obtained as

$$\frac{\partial \sigma_{q_{c,r}}^2}{\partial x_m} = \frac{\sigma_{q_{c,r}}^2 \omega_{\pi_{c,r}(m)} \prod_{\substack{i=1 \\ i \neq m}}^{N_{M_c}} \psi_{c,r,i}}{\sum_{i=1}^{N_{M_c}} \omega_{\pi_{c,r}(i)} x_i \prod_{\substack{j=1 \\ j \neq i}}^{N_{M_c}} \psi_{c,r,j}}, \quad (45)$$

where $\psi_{c,r,i} \triangleq \omega_{\pi_{c,r}(i)} x_i + \sigma_{q_{c,r}}^2$. Now, after some algebraic manipulation, the second partial derivative of $\sigma_{q_{c,r}}^2$ with respect to x_m can be expressed as

$$\begin{aligned} \frac{\partial^2 \sigma_{q_{c,r}}^2}{\partial x_m^2} &= \frac{-\sigma_{q_{c,r}}^2 \omega_{\pi_{c,r}(m)}^2 \prod_{\substack{j=1 \\ j \neq m}}^{N_{M_c}} \psi_{c,r,j}^2}{\left(\sum_{i=1}^{N_{M_c}} \omega_{\pi_{c,r}(i)} x_i \prod_{\substack{j=1 \\ j \neq i}}^{N_{M_c}} \psi_{c,r,j} \right)^2} \sum_{\substack{i=1 \\ i \neq m}}^{N_{M_c}} \frac{\omega_{\pi_{c,r}(i)} x_i}{\psi_{c,r,i}} \\ &\times \left[1 - \frac{\sigma_{q_{c,r}}^2 (\omega_{\pi_{c,r}(m)} x_m - \omega_{\pi_{c,r}(i)} x_i) \prod_{\substack{j=1 \\ j \neq i \\ j \neq m}}^{N_{M_c}} \psi_{c,r,j}}{\sum_{i=1}^{N_{M_c}} \omega_{\pi_{c,r}(i)} x_i \prod_{\substack{j=1 \\ j \neq i}}^{N_{M_c}} \psi_{c,r,j}} \right], \end{aligned} \quad (46)$$

where the terms outside the square brackets are always negative and the terms inside the square brackets are always positive, thus proving the non-convexity of $\sigma_{q_{c,r}}^2 = F(\Upsilon_c, \bar{W}_{c,r}^{(3)}, \bar{C}_{c,r})$.

REFERENCES

- [1] "Cisco visual networking index: Forecast and methodology, 2015–2020," Cisco, San Jose, CA, USA, White Paper, Jun. 2016. [Online]. Available: www.cisco.com
- [2] F. Boccardi, R. W. Heath, A. Lozano, T. L. Marzetta, and P. Popovski, "Five disruptive technology directions for 5G," *IEEE Commun. Mag.*, vol. 52, no. 2, pp. 74–80, Feb. 2014.
- [3] A. Checko *et al.*, "Cloud RAN for mobile networks—A technology overview," *IEEE Commun. Surveys Tuts.*, vol. 17, no. 1, pp. 405–426, 1st Quart., 2015.
- [4] D. Gesbert, S. Hanly, H. Huang, S. S. Shitz, O. Simeone, and W. Yu, "Multi-cell MIMO cooperative networks: A new look at interference," *IEEE J. Sel. Areas Commun.*, vol. 28, no. 9, pp. 1380–1408, Dec. 2010.
- [5] J. Jose, A. Ashikhmin, T. L. Marzetta, and S. Vishwanath, "Pilot contamination and precoding in multi-cell TDD systems," *IEEE Trans. Wireless Commun.*, vol. 10, no. 8, pp. 2640–2651, Aug. 2011.
- [6] R. Zakhour and S. V. Hanly, "Base station cooperation on the downlink: Large system analysis," *IEEE Trans. Inf. Theory*, vol. 58, no. 4, pp. 2079–2106, Apr. 2012.
- [7] A. Kamoun, A. Müller, E. Björnson, and M. Debbah, "Linear precoding based on polynomial expansion: Large-scale multi-cell MIMO systems," *IEEE J. Sel. Topics Signal Process.*, vol. 8, no. 5, pp. 861–875, Oct. 2014.
- [8] G. Nigam, P. Minero, and M. Haenggi, "Coordinated multipoint joint transmission in heterogeneous networks," *IEEE Trans. Commun.*, vol. 62, no. 11, pp. 4134–4146, Nov. 2014.
- [9] A. Lozano, R. W. Heath, Jr., and J. G. Andrews, "Fundamental limits of cooperation," *IEEE Trans. Inf. Theory*, vol. 59, no. 9, pp. 5213–5226, Sep. 2013.
- [10] J. Hoydis, K. Hosseini, S. T. Brink, and M. Debbah, "Making smart use of excess antennas: Massive MIMO, small cells, and TDD," *Bell Labs Tech. J.*, vol. 18, no. 2, pp. 5–21, Sep. 2013.
- [11] K. Hosseini, W. Yu, and R. S. Adve, "Large-scale MIMO versus network MIMO for multicell interference mitigation," *IEEE J. Sel. Topics Signal Process.*, vol. 8, no. 5, pp. 930–941, Oct. 2014.
- [12] E. Björnson, E. G. Larsson, and M. Debbah, "Massive MIMO for maximal spectral efficiency: How many users and pilots should be allocated?" *IEEE Trans. Wireless Commun.*, vol. 15, no. 2, pp. 1293–1308, Feb. 2016.
- [13] X. Zhu *et al.*, "Soft pilot reuse and multicell block diagonalization precoding for massive MIMO systems," *IEEE Trans. Veh. Technol.*, vol. 65, no. 5, pp. 3285–3298, May 2016.
- [14] H. H. Yang, G. Geraci, T. Q. S. Quek, and J. G. Andrews, "Cell-edge-aware precoding for downlink massive MIMO cellular networks," *IEEE Trans. Signal Process.*, vol. 65, no. 13, pp. 3344–3358, Jul. 2017.
- [15] F. Riera-Palou and G. Femenias, "Cluster-based cooperative MIMO-OFDMA cellular networks: Scheduling and resource allocation," *IEEE Trans. Veh. Technol.*, vol. 67, no. 2, pp. 1202–1216, Feb. 2018.
- [16] Y.-H. Nam *et al.*, "Full-dimension MIMO (FD-MIMO) for next generation cellular technology," *IEEE Commun. Mag.*, vol. 51, no. 6, pp. 172–179, Jun. 2013.
- [17] D. Ying, F. W. Vook, T. A. Thomas, D. J. Love, and A. Ghosh, "Kronecker product correlation model and limited feedback codebook design in a 3D channel model," in *Proc. IEEE Int. Conf. Commun. (ICC)*, Jun. 2014, pp. 5865–5870.
- [18] C. T. Neil, M. Shafi, P. J. Smith, and P. A. Dmochowski, "On the impact of antenna topologies for massive MIMO systems," in *Proc. IEEE Int. Conf. Commun. (ICC)*, Jun. 2015, pp. 2030–2035.
- [19] Q.-U.-A. Nadeem, A. Kamoun, M. Debbah, and M.-S. Alouini, "A generalized spatial correlation model for 3D MIMO channels based on the Fourier coefficients of power spectrums," *IEEE Trans. Signal Process.*, vol. 63, no. 14, pp. 3671–3686, Jul. 2015.
- [20] A. Adhikary, J. Nam, J.-Y. Ahn, and G. Caire, "Joint spatial division and multiplexing—The large-scale array regime," *IEEE Trans. Inf. Theory*, vol. 59, no. 10, pp. 6441–6463, Oct. 2013.
- [21] A. Alkhateeb, G. Leus, and R. W. Heath, Jr., "Multi-layer precoding: A potential solution for full-dimensional massive MIMO systems," *IEEE Trans. Wireless Commun.*, vol. 16, no. 9, pp. 5810–5824, Sep. 2017.
- [22] P. Almers *et al.*, "Survey of channel and radio propagation models for wireless MIMO systems," *EURASIP J. Wireless Commun. Netw.*, vol. 2007, no. 1, pp. 1–19, Feb. 2007.
- [23] O. El Ayach, S. Rajagopal, S. Abu-Surra, Z. Pi, and R. W. Heath, Jr., "Spatially sparse precoding in millimeter wave MIMO systems," *IEEE Trans. Wireless Commun.*, vol. 13, no. 3, pp. 1499–1513, Mar. 2014.
- [24] L. Liang, W. Xu, and X. Dong, "Low-complexity hybrid precoding in massive multiuser MIMO systems," *IEEE Wireless Commun. Lett.*, vol. 3, no. 6, pp. 653–656, Dec. 2014.
- [25] J. Kang, O. Simeone, J. Kang, and S. Shamai (Shitz), "Fronthaul compression and precoding design for C-RANs over ergodic fading channels," *IEEE Trans. Veh. Technol.*, vol. 65, no. 7, pp. 5022–5032, Jul. 2016.
- [26] J. Kang, O. Simeone, J. Kang, and S. Shamai (Shitz), "Layered downlink precoding for C-RAN systems with full dimensional MIMO," *IEEE Trans. Veh. Technol.*, vol. 66, no. 3, pp. 2170–2182, Mar. 2017.
- [27] S.-H. Park, O. Simeone, O. Sahin, and S. Shamai (Shitz), "Fronthaul compression for cloud radio access networks: Signal processing advances inspired by network information theory," *IEEE Signal Process. Mag.*, vol. 31, no. 6, pp. 69–79, Nov. 2014.
- [28] Y.-G. Lim, C.-B. Chae, and G. Caire, "Performance analysis of massive MIMO for cell-boundary users," *IEEE Trans. Wireless Commun.*, vol. 14, no. 12, pp. 6827–6842, Dec. 2015.
- [29] Z. Wang, W. Liu, C. Qian, S. Chen, and L. Hanzo, "Two-dimensional precoding for 3-D massive MIMO," *IEEE Trans. Veh. Technol.*, vol. 66, no. 6, pp. 5485–5490, Jun. 2017.
- [30] B. Dai and W. Yu, "Energy efficiency of downlink transmission strategies for cloud radio access networks," *IEEE J. Sel. Areas Commun.*, vol. 34, no. 4, pp. 1037–1050, Apr. 2016.
- [31] R. Zamir and M. Feder, "On lattice quantization noise," *IEEE Trans. Inf. Theory*, vol. 42, no. 4, pp. 1152–1159, Jul. 1996.
- [32] Z. Zhong, X. Yin, X. Li, and X. Li, "Extension of ITU IMT-advanced channel models for elevation domains and line-of-sight scenarios," in *Proc. VTC*, Sep. 2013, pp. 1–5.
- [33] N. Seifi, J. Zhang, R. W. Heath, Jr., T. Svensson, and M. Coldrey, "Coordinated 3D beamforming for interference management in cellular networks," *IEEE Trans. Wireless Commun.*, vol. 13, no. 10, pp. 5396–5410, Oct. 2014.
- [34] S. Haghighatshoar and G. Caire, "Massive MIMO channel subspace estimation from low-dimensional projections," *IEEE Trans. Signal Process.*, vol. 65, no. 2, pp. 303–318, Jan. 2017.

- [35] E. Björnson, E. G. Larsson, and T. L. Marzetta, "Massive MIMO: Ten myths and one critical question," *IEEE Commun. Mag.*, vol. 54, no. 2, pp. 114–123, Feb. 2016.
- [36] T. M. Cover and J. A. Thomas, *Elements of Information Theory* (Wiley Series in Telecommunications and Signal Processing), 2nd ed. Hoboken, NJ, USA: Wiley, 2006.
- [37] Z. Ugray, L. Lasdon, J. Plummer, F. Glover, J. Kelly, and R. Martí, "Scatter search and local NLP solvers: A multistart framework for global optimization," *INFORMS J. Comput.*, vol. 19, no. 3, pp. 328–340, 2007.
- [38] P. Kyösti *et al.*, *WINNER II Channel Models—Part I: Channel Models*, document EU FP6, Deliverable IST-4-027756 WINNER II-D1.1.2 V1.2, Sep. 2007. [Online]. Available: <http://projects.celtic-initiative.org/winner+/WINNER2-Deliverables/D1.1.2v1.1.pdf>
- [39] H. Claussen, "Efficient modelling of channel maps with correlated shadow fading in mobile radio systems," in *Proc. IEEE 16th Int. Symp. Pers., Indoor Mobile Radio Commun.*, vol. 1, Sep. 2005, pp. 512–516.



GUILLEM FEMENIAS (SM'11) received the degree in telecommunication engineering and the Ph.D. degree in electrical engineering from the Technical University of Catalonia (UPC), Barcelona, Spain, in 1987 and 1991, respectively. From 1987 to 1994, he was a Researcher with UPC, where he became an Associate Professor in 1992. In 1995, he joined the Department of Mathematics and Informatics, University of the Balearic Islands (UIB), Palma de Mallorca, Spain, where he became Full Professor in 2010. In the past, he was involved in several European projects (ATDMA, CODIT, and COST). He is currently leading the Mobile Communications Group at UIB, where he has been the Project Manager of projects ARAMIS, DREAMS, DARWIN, MARIMBA, COSMOS, ELISA, and TERESA, all of them funded by the Spanish and Balearic Islands Governments. His current research interests and activities span the fields of digital communications theory and wireless communication systems, with a particular emphasis on cross-layer transceiver design, resource management, and scheduling strategies applied to fourth- and fifth-generation wireless networks. On these topics, he has published more than 90 journal and conference papers and some book chapters. He was a recipient of the Best Paper Awards at the 2007 IFIP International Conference on Personal Wireless Communications and the 2009 IEEE Vehicular Technology Conference-Spring (VTC-Spring). He has served for various IEEE conferences as a Technical Program Committee Member, the Publications Chair for the IEEE 69th VTC-Spring in 2009, and a Local Organizing Committee Member for the IEEE Statistical Signal Processing in 2016.



FELIP RIERA-PALOU (SM'11) received the integrated B.S./M.S. degree in computer engineering from the University of the Balearic Islands (UIB), Palma de Mallorca, Spain, in 1997, the M.Sc. and Ph.D. degrees in communication engineering from the University of Bradford, U.K., in 1998 and 2002, respectively, and the M.Sc. degree in statistics from the University of Sheffield, U.K., in 2006. From 2002 to 2005, he was with Philips Research Laboratories, Eindhoven, The Netherlands, first as a Marie Curie Post-Doctoral Fellow (European Union) and then as a Member of Technical Staff. While at Philips, he worked on research programs related to wideband speech/audio compression and speech enhancement for mobile telephony. From 2005 to 2009, he was a Research Associate (Ramon y Cajal program, Spanish Ministry of Science) at the Mobile Communications Group, Department of Mathematics and Informatics, UIB. Since 2010, he has been an Associate Research Professor (I3 Program, Spanish Ministry of Education), UIB. His current research interests are in the general areas of signal processing and wireless communications.

• • •